Spin-orbit angle measurements for six southern transiting planets[*]

New insights into the dynamical origins of hot Jupiters

Amaury H.M.J. Triaud[1], Andrew Collier Cameron[2], Didier Queloz[1], David R. Anderson[3], Michaël Gillon[4], Leslie Hebb[5], Coel Hellier[3], Benoît Loeillet[6], Pierre F. L. Maxted[3], Michel Mayor[1], Francesco Pepe[1], Don Pollacco[7], Damien Ségransan[1], Barry Smalley[3], Stéphane Udry[1], Richard G. West[8], and Peter J. Wheatley[9]

[1] Observatoire Astronomique de l'Université de Genève, Chemin des Maillettes 51, CH-1290 Sauverny, Switzerland
[2] School of Physics & Astronomy, University of St Andrews, North Haugh, St Andrews KY16 9SS, Fife, Scotland, UK
[3] Astrophysics Group, Keele University, Staffordshire ST55BG, UK
[4] Institut d'Astrophysique et de Géophysique, Université de Liège, Allée du 6 Août, 17, Bat. B5C, Liège 1, Belgium
[5] Department of Physics and Astronomy, Vanderbilt University, Nashville, TN37235, USA
[6] Laboratoire dAstrophysique de Marseille, BP 8, 13376 Marseille Cedex 12, Franc
[7] Astrophysics Research Centre, School of Mathematics & Physics, Queens University, University Road, Belfast BT71NN, UK
[8] Department of Physics and Astronomy, University of Leicester, Leicester LE17RH, UK
[9] Department of Physics, University of Warwick, Coventry CV4 7AL, UK

ABSTRACT

Context. There are competing scenarii for planetary systems formation and evolution trying to explain how hot Jupiters came to be so close to their parent star. Most planetary parameters evolve with time, making distinction between models hard to do. It is thought the obliquity of an orbit with respect to the stellar rotation is more stable than other parameters such as eccentricity. Most planets, to date, appear aligned with the stellar rotation axis; the few misaligned planets so far detected are massive ($> 2 M_J$).

Aims. Our goal is to measure the degree of alignment between planetary orbits and stellar spin axes, to detect potential correlation with eccentricity or other planetary parameters and to measure long term radial velocity variability indicating the presence of other bodies in the system.

Methods. For transiting planets, the Rossiter-McLaughlin effect allows the measurement of the sky-projected angle β between the stellar rotation axis and a planet's orbital axis. Using the HARPS spectrograph, we observed the Rossiter-McLaughlin effect for six transiting hot Jupiters found by the WASP consortium. We combine these with long term radial velocity measurements obtained with CORALIE. We used a combined analysis of photometry and radial velocities, fitting models with a Markov Chain Monte Carlo. After obtaining β we attempt to statistically determine the distribution of the real spin-orbit angle ψ.

Results. We found that three of our targets have β above 90°: WASP-2b: $\beta = 153°^{+11}_{-15}$, WASP-15b: $\beta = 139.6°^{+5.2}_{-4.3}$ and WASP-17b: $\beta = 147.3°^{+5.9}_{-5.5}$; the other three (WASP-4b, WASP-5b and WASP-18b) have angles compatible with 0°. There is no dependence between the misaligned angle and planet mass nor with any other planetary parameter. All orbits are close to circular, with only one firm detection of eccentricity on WASP-18b with $e = 0.0084^{+0.0008}_{-0.0010}$. No long term radial acceleration was detected for any of the targets. Combining all previous 20 measurements of β and our six and transforming them into a distribution of ψ we find that about 80% of hot Jupiters have $\psi > 22°$.

Conclusions. Most hot Jupiters are misaligned, with a large variety of spin-orbit angles. We observe that the histogram of projected obliquities matches closely the theoretical distributions of ψ using Kozai cycles and tidal friction. If these observational facts are confirmed in the future, we may then conclude that most hot Jupiters are formed by this very mechanism without the need to use type I or II migration. At present, type I or II migration alone cannot explain the observations.

Key words. binaries: eclipsing – planetary systems – stars: individual: WASP-2, WASP-4, WASP-5, WASP-15, WASP-17, WASP-18 – techniques: spectroscopic

1. Introduction

The formation of close-in gas giant planets, the so-called *hot Jupiters*, has been in debate since the discovery of the first of them, 51 Peg b, by Mayor & Queloz (1995). The repeated observations of these planets in radial velocity and the discovery

with HD 209548b (Charbonneau et al. 2000; Henry et al. 2000) that some of them transit has produced a large diversity in planetary parameters, such as separation, mass, radius (hence density) and eccentricity. Although more than 440 extrasolar planets have been discovered, of which more than 70 are known to transit, we are still increasing the range of parameters that planets occupy; diversity keeps growing.

While it is generally accepted that close-orbiting gas-giant planets do not form in-situ, their previous and subsequent evolution is still mysterious. Several processes can affect the planet's eccentricity and semi-major axis. Inward migration via angular momentum exchange with a gas disc, first proposed in Lin et al.

(1996) from work by Goldreich & Tremaine (1980), is a natural and widely-accepted explanation for the existence of these hot Jupiters.

Migration alone does not explain the observed distributions in eccentricity and semi-major axis that planets occupy. Alternative mechanisms have therefore been proposed such as the Kozai mechanism (Kozai 1962; Eggleton & Kiseleva-Eggleton 2001; Wu & Murray 2003) and planet scattering (Rasio & Ford 1996). These mechanisms can also cause a planet to migrate inwards, and may therefore have a role to play in the formation and evolution of hot Jupiters. These different models each predict a distribution in semi-major axis and eccentricity. Discriminating between various models is done by matching the distributions they produce to observations. Unfortunately this process does not take into account the evolution with time of the distributions and is made hard by the probable combination of a variety of effects.

On transiting planets, a parameter can be measured which might prove a better marker of the past history of planets: β, the projection on the sky of the angle between the star's rotation axis and the planet's orbital axis. It is believed that the obliquity (the real spin-orbit angle ψ) of an orbit evolves only slowly and is not as much affected by the proximity of the star as the eccentricity (Hut 1981; Winn et al. 2005; Barker & Ogilvie 2009). Disc migration is expected to leave planets orbiting close to the stellar equatorial plane. Kozai cycles and planet scattering should excite the obliquity of the planet and should provide us with a planet population on misaligned orbits with respect to their star's rotation.

As a planet transits a rotating star, it will cause an overall redshifting of the spectrum if it covers the blue-shifted half of the star and vice-versa on the other side. This is called the Rossiter-McLaughlin effect (Rossiter 1924; McLaughlin 1924). It was first observed for a planet by Queloz et al. (2000). Several papers model this effect: Ohta et al. (2005); Giménez (2006); Gaudi & Winn (2007).

Among the 70 or so known transiting planets discovered since 2000 by the huge effort sustained by ground-based transiting planet searches, the Rossiter-McLaughlin (RM) effects have been measured for 20, starting with observations on HD 209458 by Queloz et al. (2000). This method has proven itself reliable at giving precise and accurate measurement of the projected spin-orbit angle with its best determination done for HD 189733b (Triaud et al. 2009). Basing their analysis on measurements of β in 11 systems, 10 of which are coplanar or nearly so, Fabrycky & Winn (2009) concluded that the angle distribution is likely to be bimodal with a coplanar population and an isotropically-misaligned population. At that time, the spin-orbit misalignment of XO-3b (Hébrard et al. 2008) comprised the only evidence of the isotropic population. Since then, the misalignment of XO-3b has been confirmed by Winn et al. (2009c), and significant misalignments have been found for HD 80606b (Moutou et al. 2009) and WASP-14b (Johnson et al. 2009). Moreover, retrograde motion orbital has been identified in HAT-P-7b (Winn et al. 2009b; Narita et al. 2009). Other systems show indications of misalignment but need confirmation. One such object is WASP-17b (Anderson et al. 2010) which is one of the subjects of the present paper.

The Wide Angle Search for Planets (WASP) project aims at finding transiting gas giants (Pollacco et al. 2006). Observing the northern and southern hemispheres with sixteen 11 cm refractive telescopes, the WASP consortium has published more than 20 transiting planets in a large range of period, mass and radius,

Table 1. List of Observations. The date indicates when the first point of the Rossiter-McLaughlin sequence was taken.

Target	Date	Instrument	Paper
WASP-18b	2008/08/21	HARPS	this paper
WASP-8b	2008/10/05	HARPS	Queloz et al. *submitted*
WASP-6b	2008/10/07	HARPS	Gillon et al. (2009a)
WASP-4b	2000/10/08	HARPS	this paper
WASP-5b	2008/10/10	HARPS	this paper
WASP-2b	2008/10/15	HARPS	this paper
WASP-15b	2009/04/27	HARPS	this paper
WASP-17b	2009/05/22	CORALIE	this paper
WASP-17b	2009/07/05	HARPS	this paper

around stars with apparent magnitudes between 9 and 13. The planet candidates observable from the South are confirmed by a large radial-velocity follow-up using the CORALIE high resolution échelle spectrograph, mounted on the 1.2 m *Euler* Swiss Telescope, at La Silla, Chile. As part of our efforts to understand the planets that have been discovered, we have initiated a systematic program to measure the Rossiter-McLaughlin effect in the planets discovered by the WASP survey, in order to measure their projected spin-orbit misalignment angles β.

In this paper we report the measurement of β in six southern transiting planets from the WASP survey, and analyse their long term radial velocity behaviour. In sections 2 and 3 we describe the observations and the methods employed to extract and analyse the data. In section 4 we report in detail on the Rossiter-McLaughlin effects observed during transits of the six systems observed. In sections 5 and 6 we discuss the correlations and trends that emerge from the study and their implications for planetary migration models.

2. The Observations

In order to determine precisely and accurately the angle β, we need to obtain radial velocities during planetary transits at a high cadence and high precision. We therefore observed with the high resolution échelle spectrograph HARPS, mounted at the La Silla 3.6 m ESO telescope. The magnitude range within which planets are found by the SuperWASP instruments allows us to observe each object in adequate conditions. For the main survey proposal 082.C-0040, we selected as targets the entire population of transiting planets known at the time of proposal submission to be observable from La Silla during Period 82, i.e. WASP-2b, 4b, 5b, 6b, 8b and 15b. The results for WASP-6b are presented separately by Gillon et al. (2009a) and for WASP-8b by Queloz et al. (*submitted*). Two targets were added in separate proposals. A transit of WASP-18b was observed during GTO time (072C-0488) of the HARPS consortium allocated to this planet because of its short and eccentric orbit. During the long-term spectroscopic follow-up of WASP-17b undertaken for the discovery paper (Anderson et al. 2010), three CORALIE measurements fell during transit showing a probably retrograde orbit. Observations of the Rossiter-McLaughlin with CORALIE confirmed the conclusions of Anderson et al. (2010), and a followup DDT proposal (283.C-5017) was awarded time on HARPS.

The strategy of observations was to take two high precision HARPS points the day before transit and the day after transit. The radial-velocity curve was sampled densely throughout the

Table 2. Stellar parameters used in our model fitting. The $v \sin I$ (stellar spectroscopic rotation broadening) and stellar mass estimates are used as priors in the analysis. ξ_t is the microturbulence. V_{macro} is the macrotrubulence.

Parameters	units	WASP-2 (a,b)	WASP-4 (c)	WASP-5 (c)	WASP-15 (d)	WASP-17 (a,e)	WASP-18 (f)
Spectral Type		K1	G8	G5	F7	F4	F6
T_{eff}	K	5150 ± 80	5500 ± 100	5700 ± 100	6300 ± 100	6650 ± 80	6400 ± 100
$\log g$		4.40 ± 0.15	4.5 ± 0.2	4.5 ± 0.2	4.35 ± 0.15	4.45 ± 0.15	4.4 ± 0.15
[Fe/H]		-0.08 ± 0.08	-0.03 ± 0.09	$+0.09 \pm 0.09$	-0.17 ± 0.11	-0.19 ± 0.09	0.00 ± 0.09
ξ_t	km s^{-1}	0.9 ± 0.1	1.1 ± 0.2	1.2 ± 0.2	1.4 ± 0.1	1.7 ± 0.1	1.6 ± 0.1
V_{macro}	km s^{-1}	1.6	2.0	2.0	4.8	6.2	4.8
$v \sin I$	km s^{-1}	1.6 ± 0.7	2.0 ± 1.0	3.5 ± 1.0	4.0 ± 2.0	9.8 ± 0.5	11.0 ± 1.5
$M_\star$	M$_\odot$	0.84 ± 0.11	0.93 ± 0.05	1.00 ± 0.06	1.18 ± 0.12	1.2 ± 0.12	1.24 ± 0.04

Note 1. references: (a) this paper, (b) Cameron et al. (2007), (c) Gillon et al. (2009c), (d) West et al. (2009), (e) Anderson et al. (2010), (f) Hellier et al. (2009)

transit, beginning 90 minutes before ingress and ending 90 minutes after egress. The data taken before ingress and after egress allow any activity-related offset in the effective velocity of the system's centre of mass to be determined for the night of observation. In addition, radial velocity data from the high resolution échelle spectrograph CORALIE mounted on the Swiss 1.2 m *Euler* Telescope, also at La Silla was acquired to help search for a long term variability in the the periodic radial velocity signal.

All our HARPS observations have been conducted in the OBJO mode, without simultaneous Thorium-Argon spectrum. HARPS is stable within 1 m s^{-1} across a week. This is lower than our individual error bars and leads to no contamination of the Th-Ar lamp onto the stellar spectrum easing spectral analysis.

3. The Data Analysis

3.1. Radial-velocity extraction

The spectroscopic data were reduced using the online Data Reduction Software (DRS) which comes with HARPS. The radial velocity information was obtained by removing the instrumental blaze function and cross-correlating each spectrum with one of two masks. This correlation is compared with the Th-Ar spectrum acting as a reference; see Baranne et al. (1996), Pepe et al. (2002) & Mayor et al. (2003) for details. Recently the DRS was shown to achieve remarkable precision (Mayor et al. 2009) thanks to a revision of the reference lines for Thorium and Argon by Lovis & Pepe (2007). Stars with spectral type earlier than G9 were reduced using the G2 mask, while those of K0 or later were cross-correlated with the K5 mask. A similar software package is used for CORALIE data. A resolving power $R = 110\,000$ for HARPS yields a cross-correlation function (CCF) binned in 0.25 km s^{-1} increments, while for CORALIE, with a lower resolution of 50 000, we used 0.5 km s^{-1}. The CCF window was adapted to be three times the size of the full width at half maximum (FWHM) of the CCF.

All our past and current CORALIE data on the stars presented here were reprocessed after removal of the instrumental blaze response, thereby changing slightly some radial velocity values compared to those already published in the literature. Correcting this blaze is important for extracting the correct RVs for the RM effect. The uncorrected blaze created a slight systematic asymmetry in the CCF that was translated into a bias in radial velocities.

1 σ error bars on individual data points were estimated from photon noise alone. HARPS is stable long term within 1 m s^{-1} and CORALIE at less than 5 m s^{-1}. These are smaller than our individual error bars and thus have not been taken into account.

3.2. Spectral analysis

Spectral analysis is needed to determine the stellar atmospheric parameters from which limb darkening coefficients can be inferred. We carried out new analyses for two of the target stars, WASP-2 and WASP-17, whose previously-published spectroscopic parameters were of low precision. For our other targets, the atmospheric parameters were taken from the literature, notably the stellar spectroscopic rotation broadening $v \sin I$ [1].

The individual HARPS spectra can be co-added to form an overall spectrum above S/N ~ 1 : 100, suitable for photospheric analysis which was performed using the UCLSYN spectral synthesis package (Smith 1992; Smalley et al. 2001) and ATLAS9 models without convective overshooting (Castelli et al. 1997) and the same method as described in many discovery papers published by the WASP consortium (eg: Wilson et al. (2008)).

The stellar rotational $v \sin I$ is determined by fitting the profiles of several unblended Fe I lines. The instrumental FWHM was determined to be 0.065Å from the telluric lines around 6300Å.

For WASP-2, a value for macroturbulence (v_{mac}) of 1.6 km s^{-1} was adopted (Gray 2008). A best fitting value of $v \sin I = 1.6 \pm 0.7$ km s^{-1} was obtained. On WASP-17, a value for macroturbulence (v_{mac}) of 6.2 km s^{-1} was used (Gray 2008). The analysis gives a best fitting value of $v \sin I = 9.8 \pm 0.5$ km s^{-1}.

All stellar parameters, used as well as derived, are presented in Table 2.

3.3. Model fitting

The extracted radial velocity data was fitted simultaneously with the transit photometry available at the time of analysis. Three

---

[1] throughout this paper we use the symbol I to denote the inclination of the stellar rotation axis to the line of sight, while i represents the inclination of the planet's orbital angular momentum vector to the line of sight

models are adjusted to the data: a Keplerian radial velocity orbit (Hilditch 2001), a photometric planetary transit (Mandel & Agol 2002), and a spectroscopic transit, also known as Rossiter-McLaughlin effect (Giménez 2006). This combined approach is very useful for reducing the total number of free parameters and to ensure that the fitted model is fully consistent with the various datasets. A single set of parameters describes both the photometry and the radial velocities. We use a Markov Chain Monte Carlo (MCMC) approach to optimize the models and estimate the uncertainties of the fitted parameters. The fit of the model to the data is quantified using the χ^2 statistic.

The code is described in detail by Triaud et al. (2009), has been used several times (eg: Gillon et al. (2009a)) and is similar to the code described in Cameron et al. (2007).

We fitted up to 10 parameters, namely the depth of the primary transit D, the radial velocity (RV) semi-amplitude K, the impact parameter b, the transit width W, the period P, the epoch of mid-transit T_0, $e \cos \omega$, $e \sin \omega$, $V \sin I \cos \beta$, and $V \sin I \sin \beta$. Here e is the eccentricity and ω the angle between the line of sight and the periastron, $V \sin I$ is the sky-projected rotation velocity of the star[2] while β is the sky-projected angle between the stellar rotation axis (Hosokawa 1953; Giménez 2006) and the planet's orbital axis[3].

These parameters have been chosen to reduce correlations between then. Reducing correlations means the code runs faster since it prevents us from exploring useless portions of parameter space. Eccentricity and periastron angle were paired as were $V \sin I$ and β. This breaks a correlation between them (the reader is invited to compare Figs. 2d & 3 for a clear illustration for choosing certain jump parameters as opposed to others). This way we also explore solutions around zero more easily: $e \cos \omega$ and $e \sin \omega$ move in the]-1,1[range while e could only be floating in]0,1[. For exploring particular solutions such as a circular orbit, parameters can be fixed to certain values.

In addition to the physical free floating parameters, we need to use one γ velocity for each RV set and one normalisation factor for each lightcurve as adjustment parameters. These are found by using optimal averaging and optimal scaling. γ velocities represent the mean radial velocity of the star in space with respect to the barycentre of the Solar System. Since our analysis had many datasets, the results for these adjustment parameters have been omitted, not adding anything to the discussion.

During these initial analyses we also fitted an additional acceleration in the form of an RV drift $\dot{\gamma}$ but on no occasion was it significantly different from zero. We therefore assumed there was no drift for any of our objects. We will give upper limits for each star in the following sections.

The MCMC algorithm perturbs the fitting parameters at each step i with a simple formula:

$$P_{i,j} = P_{i-1,j} + f \, \sigma_{P_j} \, G(0,1) \tag{1}$$

where P_j is a free parameter, G is a Gaussian random number of unit standard deviation and zero mean, while σ is the step size for each parameter. A factor f is used to control the chain and ensures that 25 % of steps are being accepted via a Metropolis-Hastings algorithm, as recomended in Tegmark et al. (2004) to give an optimal exploration of parameter space.

---

[2] we make a distinction between $v \sin I$ and $V \sin I$: $v \sin I$ is the value extracted from the spectral analysis, the stellar spectroscopic rotation broadening, while $V \sin I$ denotes the result of a Rossiter-McLaughlin effect fit. Both can at times be different. Each, although caused by the same effect, is independently measured making the distinction worthwhile.

[3] $\beta = -\lambda$, another notation used in the literature for the same angle.

The step size is adapted by doing several initial analyses. They are adjusted to produce as small a correlation length as possible. Once the value is chosen, it remains fixed. Only f fluctuates.

A *burn-in* phase of 50 000 accepted steps is used to make the chain converge. This is detected when the correlation length of each parameter is small and that the average χ^2 does not improve anymore (Tegmark et al. 2004). Then starts the real chain, of 500 000 accepted steps, from which results will be extracted. This number of steps is used as a compromise between computation time and exploration. 500 000 steps really represents a parameter space exploration between 4 and 5 σ around the solution. Nevertheless statistical tests, notably by comparing χ^2 can be used to estimate significance above 5 σ.

Bayesian penalties acting as prior probability distribution can be added to χ^2 to account for any prior information that we might have on any fitted or derived parameter. Stellar mass $M_\star$ can notably be inserted via a prior in the MCMC in order to propagate its error bars on the planet's mass. We also inserted the $v \sin I$ found by spectral analysis as priors in some of our fits to control how much the fit was dependent on them and the resulting value of $V \sin I$ and whether this influenced the fitted value of β. The prior values are in Table 2.

We use a quadratic limb-darkening law with fixed values for the two limb darkening coefficients appropriate to the stellar effective temperature. They were extracted for the photometry from tables published in Claret (2000). For the radial velocity (the Rossiter-McLaughlin effect is also dependent on limb darkening) we use values for the V band. Triaud et al. (2009) showed that HARPS is centred on the V band. The coefficients were chosen for atmospheric parameters close to those presented in Table 2.

3.4. Extracting the results

For each star, we performed four analyses, each using a MCMC chain with 500 000 accepted steps:

 – 1. a prior is imposed on $V \sin I$, eccentricity is fixed to zero;
 – 2. no prior on $V \sin I$, eccentricity is fixed to zero;
 – 3. a prior is imposed on $V \sin I$, eccentricity is let free;
 – 4. no prior on $V \sin I$, eccentricity is let free.

This is to assess the sensitivity of the model parameters to a small but uncertain orbital eccentricity and to the $v \sin I$ value found by spectral analysis which, as demonstrated in Triaud et al. (2009), can seriously affect the fitting of the Rossiter-McLaughlin effect. The comparative tables holding the results of these various fits are available in the appendices to support the conclusions we reach while allowing readers to form their own opinion. Our results are presented in Table 3.

The best solution is found in the best of the four fits by comparing χ^2 and using Ockham's principle of minimising the number of parameters for similar results: for fits with similar $\chi^2_{\rm reduced}$ we usually choose a circular solution with no prior on $V \sin I$. Results are extracted from the best fit by taking the median of the posterior probability distribution for each parameter, determined from the Markov chain. Errors bars are estimated from looking at the extremes of the distribution comprising the 68.3 % of the accepted steps. The best solution is not taken from the lowest χ^2 as it is dependent on the sampling and chance encounter of a - small - local minimum. Scatter plots will be presented with the positions of the best χ^2, the average and the median for illustration.
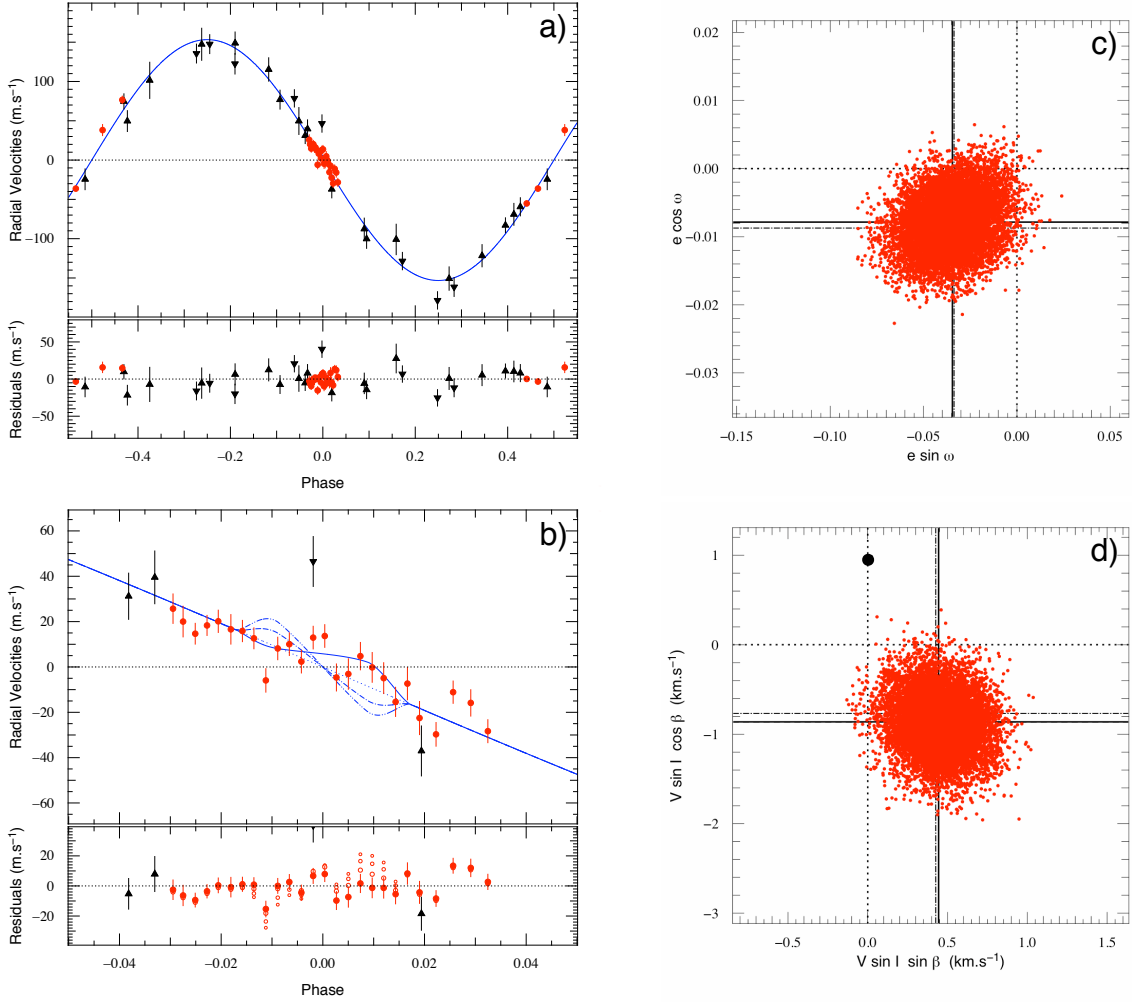
Fig. 1. Fit results for WASP-2b. *a)* Overall Doppler shift reflex motion of the star due to the planet and residuals. *b)* Zoom on the Rossiter-McLaughlin effect and residuals. Black inverted triangles are SOPHIE data, black triangles represent CORALIE points, red dots show the HARPS data. The best fit model is also pictured as a plain blue line. In addition to our best model found with $V \sin I = 0.99$ km s^{-1} we also present models with no RM effect plotted as a dotted blue line, RM effect with $\beta = 0$ and $V \sin I = 0.9$ km s^{-1} drawn with a dashed-dotted blue line and RM effect with $\beta = 0$ and $V \sin I = v \sin I = 1.6$ km s^{-1} pictured with a dashed-double dotted blue line. In the residuals, the open symbols represent in the values with the size of the circle decreasing with the likelyhood of the model. *c)* Posterior probability distribution issued from the MCMC showing the distribution of points between $e \cos \omega$ and $e \sin \omega$. *d)* Posterior probability distribution issued from the MCMC showing the distribution of points between $V \sin I \cos \beta$ and $V \sin I \sin \beta$. The **black disc** shows where the distribution would be centred for the same $V \sin I$ but with $\beta = 0$. The dotted line shows where zero is. The straight lines represent the median of the distribution, the dashed lines plot the position of the average values, the dash-dotted lines indicate the values with the lowest χ^2 (some lines can overlap). The size of boxes *c)* and *d)* represents 7 times the 1σ distance on either side of the median.

In the following section and in tables, several statistical values are used: χ^2 is the value found for all the data, while χ^2_{RV} gives the value of χ^2 solely for the radial velocities. The reduced χ^2 for the radial velocities, denoted by $\chi^2_{\mathrm{reduced}}$, is used to estimate how well a model fits the data and to compare various fits and their respective significance. In addition we will also use the residuals, denoted as $O - C$. These estimates are only for radial velocities. The results from photometry are not mentioned since they are not new. They are only here to constrain the shape of the Rossiter-McLaughlin effect.

When giving bounds, for eccentricity and long term radial velocity drift, we quote the 95% confidence interval for exclusion.

4. The Survey Results

4.1. WASP-2b

A sequence of 26 RV measurements was taken on WASP-2 using HARPS on 2008 October 15, with additional observations made outside transit as given in the journal of observations presented in the appendices. The cadence during transit was close to a point every 430s. The average photon noise error of that sequence is 5.7 m s^{-1}. We made additional observations with CORALIE to refine the orbital solution obtained by Cameron et al. (2007) using the SOPHIE instrument on the 1.93 m telescope at Observatoire de Haute-Provence, and to look for long-term variability of the orbit. 20 measurements were taken with a mean precision of 13.9 m s^{-1} over close to 11 months between 2008 October 25 and 2009 September 23. All the RV data is available in the appendices along with exposure times.
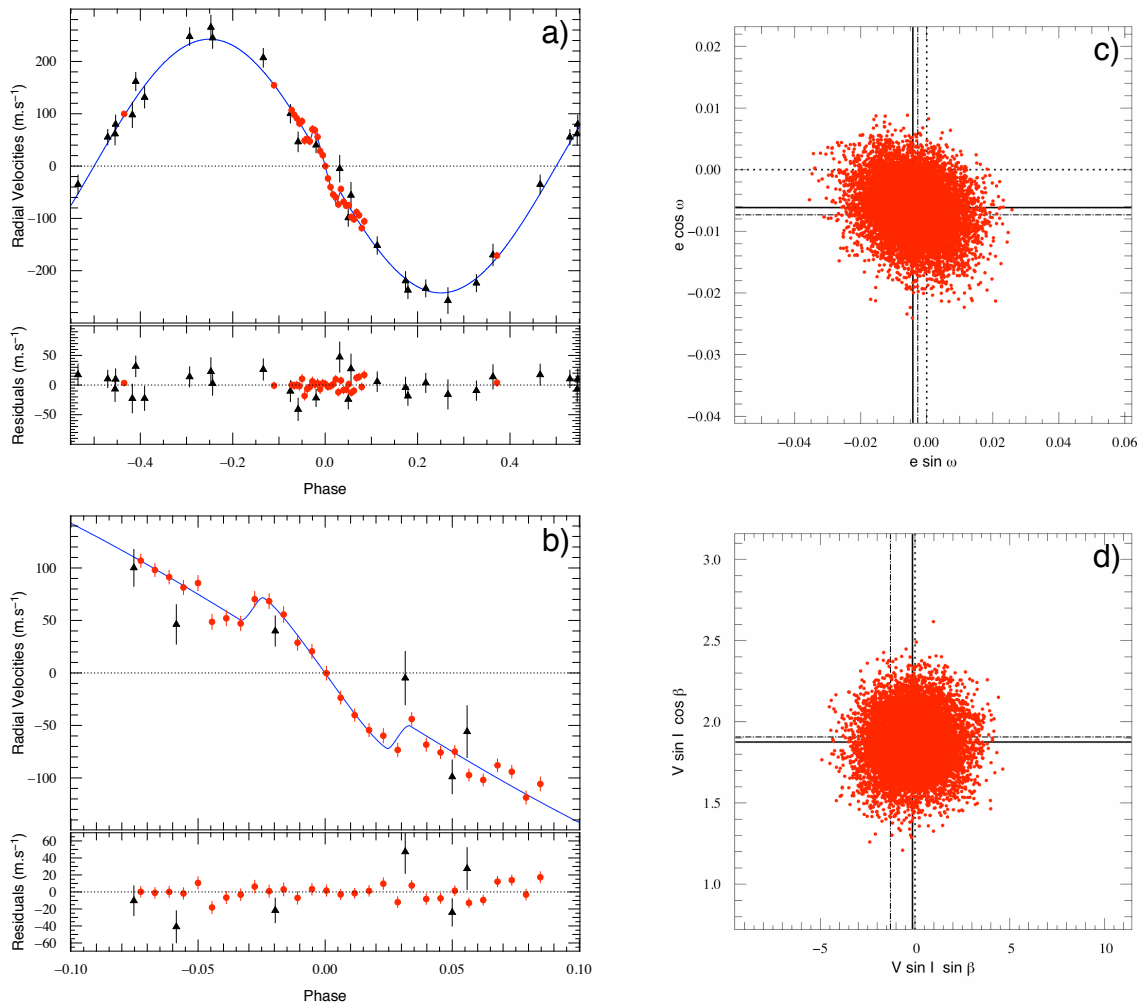
Fig. 2. Fit results for WASP-4b. *Nota Bene*: Legend similar to the legend in Fig.1.

To establish the photometric ephemeris and the transit geometry, we fitted the photometric datasets of Cameron et al. (2007) (3 seasons by SuperWASP in the unfiltered WASP bandpass), Charbonneau et al. (2007) (a *z* band *Keplercam* lightcurve) and Hrudková et al. (2009) (a William Herschel Telescope *AG2 R* band transit curve).

WASP-2b's data were fitted with up to 10 free parameters plus 8 independent adjustment parameters: three γ velocities for the three RV data sets and five normalisation factors for photometry. This sums up to 58 RV measurements and 8951 photometric observations.

χ^2_{reduced} does not improve significantly between circular and eccentric models. We therefore impose a circular solution. The presence of a prior on $V \sin I$ does not affect the results. We find $V \sin I = 0.99^{+0.27}_{-0.32}$ km s^{-1} in accordance with the $v \sin I$ value found in section 3.2. The fit delivers $\beta = 153°^{+11}_{-15}$. The overall root-mean-square (RMS) scatter of the spectroscopic residuals about the fitted model is 11.73 m s^{-1}. During the HARPS transit sequence these residuals are at 6.71 m s^{-1}.

A χ^2_{RV} comparison shows that $V \sin I$ is detected a little above the 3σ level and that β is clearly detected, at 5.6σ from an aligned solution. We have computed 6 additional chains in order to test the strength of our conclusions. Table A.1 shows the

comparison between the various fits; we invite the reader to refer to it as only important results are given in the text.

In all cases, eccentricity is not detected being below a 3σ significance from circular which is likely affected from the poor coverage of the phase by the HARPS points. Circular solutions are therefore adopted. We fix the eccentricity's upper limit to $e < 0.070$. In addition no significant long term drift was detected in the spectroscopy: $|\dot{\gamma}| < 36$ m s^{-1} yr^{-1}.

Using the spectroscopically-determined $v \sin I$ value of 1.6 km s^{-1} and forcing β to zero, χ^2_{reduced} changes from 2.14±0.27 to 3.49 ± 0.39, clearly degrading the solution. We are in fact 7.6σ away from the best-fitting solution, therefore excluding an aligned system with this large a $V \sin I$. This is also excluded by comparison to a fit with a flat RM effect at the 6.7σ. Similarly, a fit with an imposed $V \sin I = 0.9$ km s^{-1} and aligned orbit is found 5.6σ from our solution. On Fig 1b, we have plotted the various models tested and their residuals so as to give a visual demonstration of the degradation for each of the alternative solutions.

Summarising our results, we exclude the presence of an aligned Rossiter-McLaughlin effect with a $V \sin I > 0.9$ km s^{-1}. We are left to decide between only two possibilities: there is no RM effect, or there is one. The spectral line broadening shows the star rotates; an RM effect must occur. Since no aligned solution within 1σ of the spectroscopically found $v \sin I$ is valid, it

prompts the necessity of letting β float. Our misaligned solution is therefore valid.

4.2. WASP-4b

We obtained a RM sequence of WASP-4b with HARPS on 2008 October 8; other, out of transit, measurements are reported in the journal of observations given in the appendices. The RM sequence comprises 30 data points, 13 of which are in transit, taken at a cadence of 630 s^{-1} with a mean precision of 6.4 m s^{-1}. The spectrograph CORALIE continued monitoring WASP-4 and we add ten radial velocity measurements to the ones published in Wilson et al. (2008). These new data were observed around the time of the HARPS observations, about a year after spectroscopic follow-up started.

In photometry we gathered 2 timeseries in the WASP bandpass from Wilson et al. (2008) and an *R* band *C2 Euler* transit plus a *VLT/FORS2 z* band lightcurve obtained from Gillon et al. (2009c) to establish the transit shape and timing.

The WASP-4b data were fitted with up to 10 free parameters to which 6 adjustment parameters were added: two γ velocities for RVs and four normalisation factors for the photometry. In total, this represents 56 radial velocity points and 9989 photometric measurements. Gillon et al. (2009c) let combinations of limb darkening coefficients free to fit the high precision *VLT* curve. We used and fixed our coefficients on their values.

Because the impact parameter is small, a degeneracy between β and $V \sin I$ appeared, as expected (see Figs. 2d & 3). The values on stellar rotation for our unconstrained fits reach unphysical values as high as $V \sin I = 150$ km s^{-1}. We imposed a prior on the stellar rotation to restrict it to values consistent with the spectroscopic analysis.

The reduced χ^2 is the same within error bars whether eccentricity if fitted or fixed to zero. Therefore the current best solution, by minimising the number of parameters, is a circular orbit.

The eccentricity is constrained to $e < 0.0182$. Thanks to the long time series in spectroscopy we also investigated the presence of a long term radial velocity trend. Nothing was significantly detected: $|\dot{\gamma}| < 30$ m s^{-1} yr^{-1}.

Because of the small impact parameter the spin-orbit angle is poorly constrained with $\beta = -4°\,^{+43}_{-34}$, even when a prior is imposed on $V \sin I$. The high S/N of the Rossiter-McLaughlin effect allows us to exclude a projected retrograde orbit.

4.3. WASP-5b

Using HARPS, we took a series of 28 exposures on WASP-5 at a cadence of roughly 630s with a mean photon noise of 5.5 m s^{-1} on 2008 October 16. Other measurements were obtained at dates before and after this transit. Five additional CORALIE spectra were acquired the month before the HARPS observations. They were taken about a year after the data published in Anderson et al. (2008). All spectroscopic data is available from the appendices.

To help determine transit parameters, published photometry was assembled and comprises three seasons of WASP data, two *C2 Euler* lightcurves in *R* band, and one *FTS i′* band lightcurve (Anderson et al. 2008).

WASP-5b's 49 RV measurements and 14 754 photometric points were fitted with up to 10 free parameters to which 8 adjustment parameters had to be added: two γ velocities and six normalisation factors.
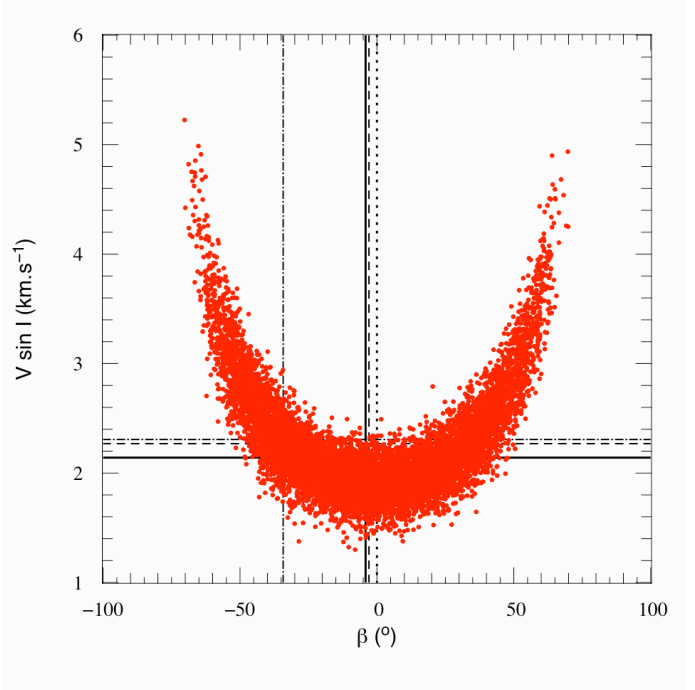

Fig. 3. Posterior probability distribution issued from the MCMC for WASP-4b showing the resulting distribution of points between $V \sin I$ and β. This distribution is issued from the chain that gave our preferred solution: a circular orbit and a prior on $V \sin I$. The dotted line shows where zero is, the straight lines represent the median of the distribution, the dashed lines plot the position of the average values, the dash-dotted lines indicate the values with the lowest χ^2 (some lines can overlap). The size of the box was adapted to include the whole distibution

The imposition of a prior on $V \sin I$ prior makes little difference to the fitted value, indicating that it is well-constrained by the data. We therefore chose not to impose the prior, thereby obtaining an independent measurement of the projected stellar equatorial rotation speed. Allowing eccentricity to float did not produce a significantly better fit. It has a 99.6 % chance of being different from zero: at 2.9 σ. Thus, minimising the number of parameters for a similar fit, we chose the solution with a circular orbit and simply place an upper limit on the eccentricity: $e < 0.0371$. No long term RV trend appears at this date: $|\dot{\gamma}| < 47$ m s^{-1} yr^{-1}.

Parameters extracted are similar to those that were published in Gillon et al. (2009c) & Anderson et al. (2008). The projection of the spin-orbit angle is found to be: $\beta = -12.4°\,^{+11.9}_{-8.2}$ and we obtain an independent measurement of $V \sin I = 3.24^{+0.34}_{-0.35}$ km s^{-1} fully compatible with the spectral value that was used as a prior in other fits. Results are presented in Table 3.

The $\chi^2_{\rm reduced}$ for spectroscopy (see Table A.1) is quite large, at 3.68 ± 0.44. The O-C for CORALIE data stand at 17.94 m s^{-1} to be compared with an average error bar of 18.13 m s^{-1}. The badness of fit therefore comes from the HARPS sequence which has a dispersion of 7.72 m s^{-1} for an average error bar of 5.49 m s^{-1}. From Fig. 4b we can see that residuals are quite important during the transit; Fig. 4d also shows that the MCMC does not find one clear solution but no better solution can be adjusted to the data: we remind that the RM effect is fitted in combination with six photometric sets which strongly constrain the impact parameter, depth and width of the Rossiter-McLaughlin effect. The radial-velocity dispersion about the model is the same out of transit as inside transit. This indicates that we do not over-fit, something

Table 3. Fitted and physical parameters found after fitting photometric and spectroscopic data of WASP-4b with a prior on $V \sin I$. The value from eccentricity was found using information from other fits as explained in the text.

| Parameters	units	WASP-2b	WASP-4b	WASP-5b	WASP-15b	WASP-17b	WASP-18b
fitted parameters							
D		$0.01802^{+0.00027}_{-0.00025}$	$0.023334^{+0.000044}_{-0.000072}$	$0.01221^{+0.00042}_{-0.00015}$	$0.00969^{+0.00013}_{-0.00011}$	$0.01669^{+0.00022}_{-0.00016}$	$0.00909^{+0.00017}_{-0.00013}$
K	m s^{-1}	$153.6^{+3.0}_{-3.1}$	$242.1^{+2.8}_{-3.1}$	$268.7^{+1.7}_{-1.9}$	$64.6^{+1.20}_{-1.25}$	$52.7^{+2.8}_{-3.1}$	$1816.9^{+1.9}_{-2.0}$
b	$R_\star$	$0.737^{+0.012}_{-0.13}$	$0.051^{+0.023}_{-0.049}$	$0.36^{+0.13}_{-0.07}$	$0.525^{+0.037}_{-0.028}$	$0.392^{+0.052}_{-0.040}$	$0.484^{+0.064}_{-0.045}$
W	days	$0.07372^{+0.00065}_{-0.00013}$	$0.08868^{+0.00008}_{-0.00006}$	$0.0988^{+0.0014}_{-0.0006}$	$0.1547^{+0.00012}_{-0.0009}$	$0.1849^{+0.0015}_{-0.001}$	$0.09056^{+0.00080}_{-0.00049}$
P	days	$2.1522254^{+0.0000008}_{-0.00000015}$	$1.3382299^{+0.0000014}_{-0.0000023}$	$1.6284229^{+0.0000044}_{-0.0000039}$	$3.752100^{+0.000009}_{-0.000009}$	$3.7354332^{+0.0000080}_{-0.0000080}$	$0.9414529^{+0.00000091}_{-0.00000074}$
T_0	bjd	$3991.51428^{+0.00020}_{-0.00021}$	$4387.327787^{+0.000040}_{-0.000039}$	$4373.99601^{+0.00015}_{-0.00014}$	$4584.69819^{+0.00020}_{-0.00020}$	$4559.18098^{+0.00026}_{-0.00026}$	$4664.90531^{+0.00016}_{-0.00017}$
$e \cos \omega$		-	-	-	-	-	$-0.0004^{+0.0007}_{-0.0075}$
$e \sin \omega$		-	-	-	-	-	$-0.0083^{+0.0010}_{-0.0008}$
$V \sin I \cos \beta$		$-0.86^{+0.30}_{-0.32}$	$1.88^{+0.18}_{-0.16}$	$3.08^{+0.44}_{-0.67}$	$-3.24^{+0.27}_{-0.36}$	$-8.47^{+0.49}_{-0.61}$	$14.60^{+0.84}_{-0.80}$
$V \sin I \sin \beta$		$0.44^{+0.17}_{-0.18}$	$-0.13^{+1.65}_{-1.33}$	$-0.70^{+0.26}_{-0.46}$	$2.75^{+0.34}_{-0.36}$	$5.44^{+0.97}_{-1.10}$	$-1.27^{+0.68}_{-0.68}$
derived parameters							
$R_{\rm p}/R_\star$		$0.1342^{+0.0010}_{-0.0009}$	$0.15275^{+0.00014}_{-0.00024}$	$0.1105^{+0.0019}_{-0.0007}$	$0.09842^{+0.00006}_{-0.00058}$	$0.12917^{+0.00085}_{-0.00062}$	$0.09532^{+0.00089}_{-0.00070}$
$R_\star/a$		$0.1248^{+0.0025}_{-0.0024}$	$0.18079^{+0.00037}_{-0.00040}$	$0.182^{+0.013}_{-0.004}$	$0.1342^{+0.0039}_{-0.0027}$	$0.1462^{+0.0041}_{-0.0062}$	$0.305^{+0.013}_{-0.008}$
$\rho_\star$	$\rho_\odot$	$1.491^{+0.088}_{-0.85}$	$1.2667^{+0.0077}_{-0.0084}$	$0.84^{+0.07}_{-0.15}$	$0.394^{+0.024}_{-0.032}$	$0.308^{+0.017}_{-0.025}$	$0.533^{+0.042}_{-0.051}$
$R_\star$	$R_\odot$	$0.825^{+0.042}_{-0.082}$	$0.903^{+0.016}_{-0.019}$	$1.056^{+0.080}_{-0.029}$	$1.440^{+0.064}_{-0.057}$	$1.574^{+0.071}_{-0.063}$	$1.324^{+0.063}_{-0.031}$
$M_\star$	$M_\odot$	$0.84^{+0.11}_{-0.040}$	$0.930^{+0.054}_{-0.053}$	$1.000^{+0.063}_{-0.067}$	$1.18^{+0.14}_{-0.12}$	$1.20^{+0.12}_{-0.12}$	$1.24^{+0.04}_{-0.04}$
$V \sin I$	km s^{-1}	$0.99^{+0.27}_{-0.32}$	$2.14^{+0.38}_{-0.35}$	$3.24^{+0.34}_{-0.35}$	$4.27^{+0.26}_{-0.36}$	$10.14^{+0.58}_{-0.79}$	$14.67^{+0.81}_{-0.57}$
$R_{\rm p}/a$		$0.01675^{+0.00045}_{-0.00040}$	$0.027617^{+0.000064}_{-0.000083}$	$0.0201^{+0.0017}_{-0.0006}$	$0.01321^{+0.00047}_{-0.00030}$	$0.01888^{+0.00062}_{-0.00039}$	$0.0291^{+0.0014}_{-0.0009}$
$R_{\rm p}$	R_J	$1.077^{+0.055}_{-0.058}$	$1.341^{+0.023}_{-0.029}$	$1.14^{+0.10}_{-0.04}$	$1.379^{+0.067}_{-0.058}$	$1.977^{+0.095}_{-0.079}$	$1.228^{+0.055}_{-0.036}$
$M_{\rm p}$	M_J	$0.866^{+0.086}_{-0.084}$	$1.250^{+0.056}_{-0.051}$	$1.555^{+0.040}_{-0.070}$	$0.551^{+0.040}_{-0.038}$	$0.453^{+0.040}_{-0.042}$	$10.11^{+0.22}_{-0.23}$
a	AU	$0.0307^{+0.0013}_{-0.015}$	$0.02320^{+0.00044}_{-0.00045}$	$0.02709^{+0.00056}_{-0.00070}$	$0.0499^{+0.0019}_{-0.0017}$	$0.0501^{+0.0016}_{-0.0018}$	$0.02019^{+0.00022}_{-0.00022}$
i	°	$84.73^{+0.8}_{-0.19}$	$89.47^{+0.51}_{-0.24}$	$86.2^{+0.8}_{-1.7}$	$85.96^{+0.29}_{-0.41}$	$86.71^{+0.38}_{-0.54}$	$81.6^{+1.0}_{-1.5}$
e		< 0.070	< 0.0182	< 0.0371	< 0.087	< 0.126	$0.0084^{+0.0008}_{-0.0010}$
ω	°	-	-	-	-	-	$-92.8^{+5.2}_{-3.9}$
β	°	153^{+11}_{-15}	-4^{+43}_{-34}	$-12.4^{+11.9}_{-8.2}$	$139.6^{+5.2}_{-4.3}$	$147.3^{+5.9}_{-5.5}$	$-5.0^{+3.1}_{-2.8}$
$|\gamma|$	(m s^{-1} yr^{-1})	< 36	< 30	< 47	< 11	< 18	$<$
O-C$_{\rm RV}$	m s^{-1}	11.73	15.16	12.70	10.89	31.33	14.00
O-C$_{\rm RM}$	m s^{-1}	6.71	6.71	7.72	6.94	$21.00; 31.27$	15.35
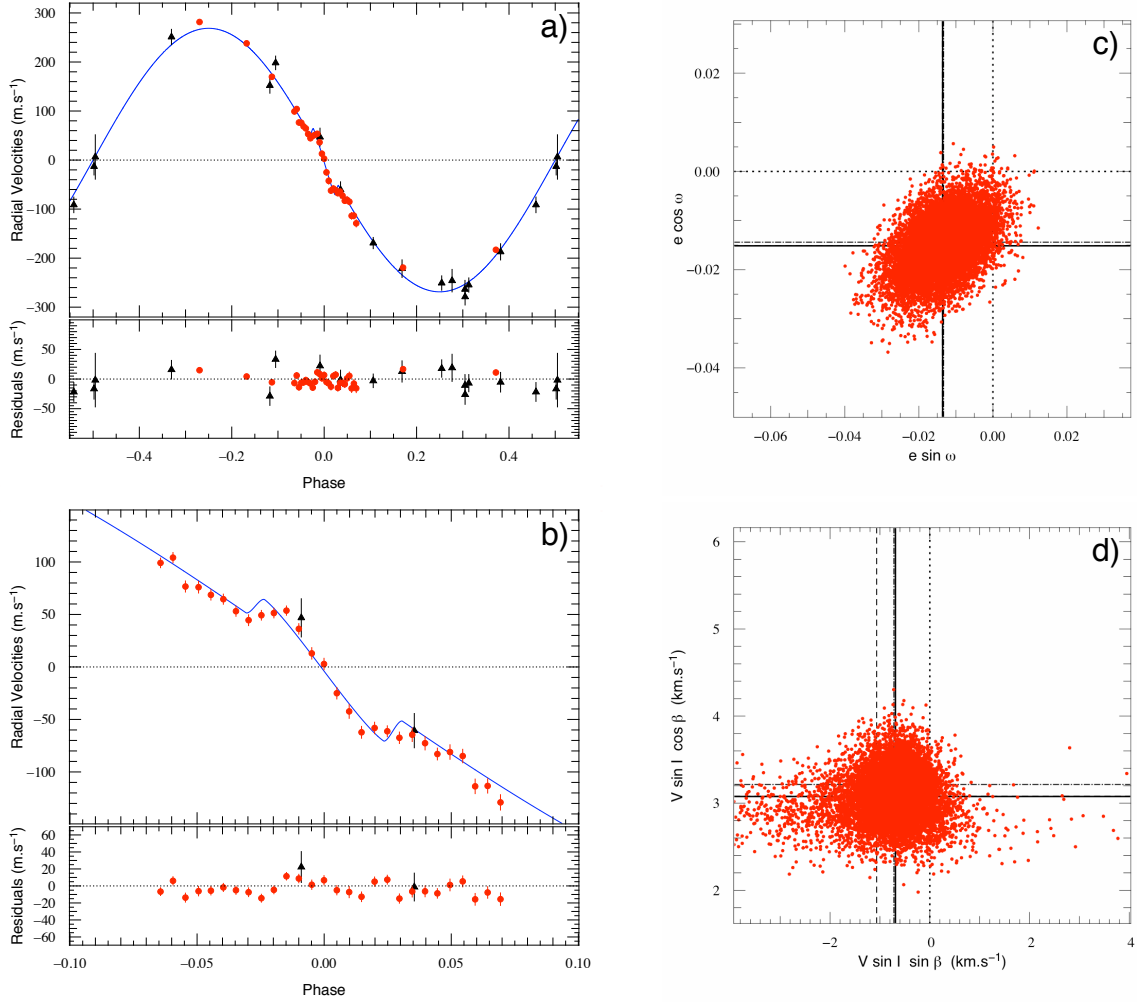
Fig. 4. Fit results for WASP-5b. *Nota Bene*: Legend similar to the legend in Fig.1.

that might happen if the RM effect were fitted on its own. The $V \sin I \cos \beta$ vs $V \sin I \sin \beta$ distribution is not centred on zero but close to it. This may come from the intrinsic dispersion in the data. A likely cause to explain the data dispersion is stellar activity.

4.4. WASP-15b

Observations were conducted using the spectrographs CORALIE and HARPS. 23 new spectra have been acquired with CORALIE in addition to the 21 presented in West et al. (2009) and extending the time series from about a year to 500 days. We observed a transit with HARPS on 2009 April 27. 46 spectra were obtained that night, 32 of which are during transits with a cadence of 430s. Additional observations have been taken as noted in the journal of observations.

The photometric sample used for fitting the transit has data from five time-series in the WASP bandpass, as well as one *I* and one *R* band transit from *C2 Euler* (West et al. 2009). The spectral data were partitioned into two sets: CORALIE and HARPS.

7 normalisation factors and 2 γ velocities were added to ten free floating parameters to adjust our models to the data which included a total of 95 spectroscopic observations and 23 089 photometric measurements.

For the various solutions attempted, χ^2_{reduced} are found the same (Table A.2). We therefore choose the priorless, circular adjustment as our solution.

Compared to West et al. (2009), parameters have only changed little. Thanks to the higher number of points we give an upper limit on eccentricity: $e < 0.087$ (Fig. 5c shows results consistent with zero); there is no evident long term evolution in the radial velocities, which is constrained within: $|\dot{\gamma}| < 11 \, \text{m s}^{-1} \, \text{yr}^{-1}$. The projected spin-orbit angle is found rather large with $\beta = 139.6°^{+5.2}_{-4.3}$ making WASP-15b appear as a retrograde planet with a very clear detection. $V \sin I$ is found within 1σ of the spectrally analysed value of $v \sin I$ from West et al. (2009) at $4.27^{+0.26}_{-0.36} \, \text{km s}^{-1}$ and as such constitutes a precise independent measurement.

$\chi^2_{\text{reduced}} = 1.51 \pm 0.19$ for the spectroscopy, indicating a good fit of the Keplerian as well as of the Rossiter-McLaughlin effect, the best fit in this paper. Full results can be seen in Table 3.

4.5. WASP-17b

On 2009 May 22, 11 CORALIE spectra were obtained at a cadence of 2030s with an average precision of 33.67 m s^{-1} to confirm the detection of retrograde orbital motion announced by Anderson et al. (2010). The sequence was stopped when airmass reached 2. HARPS was subsequently used and on 2009 July 5
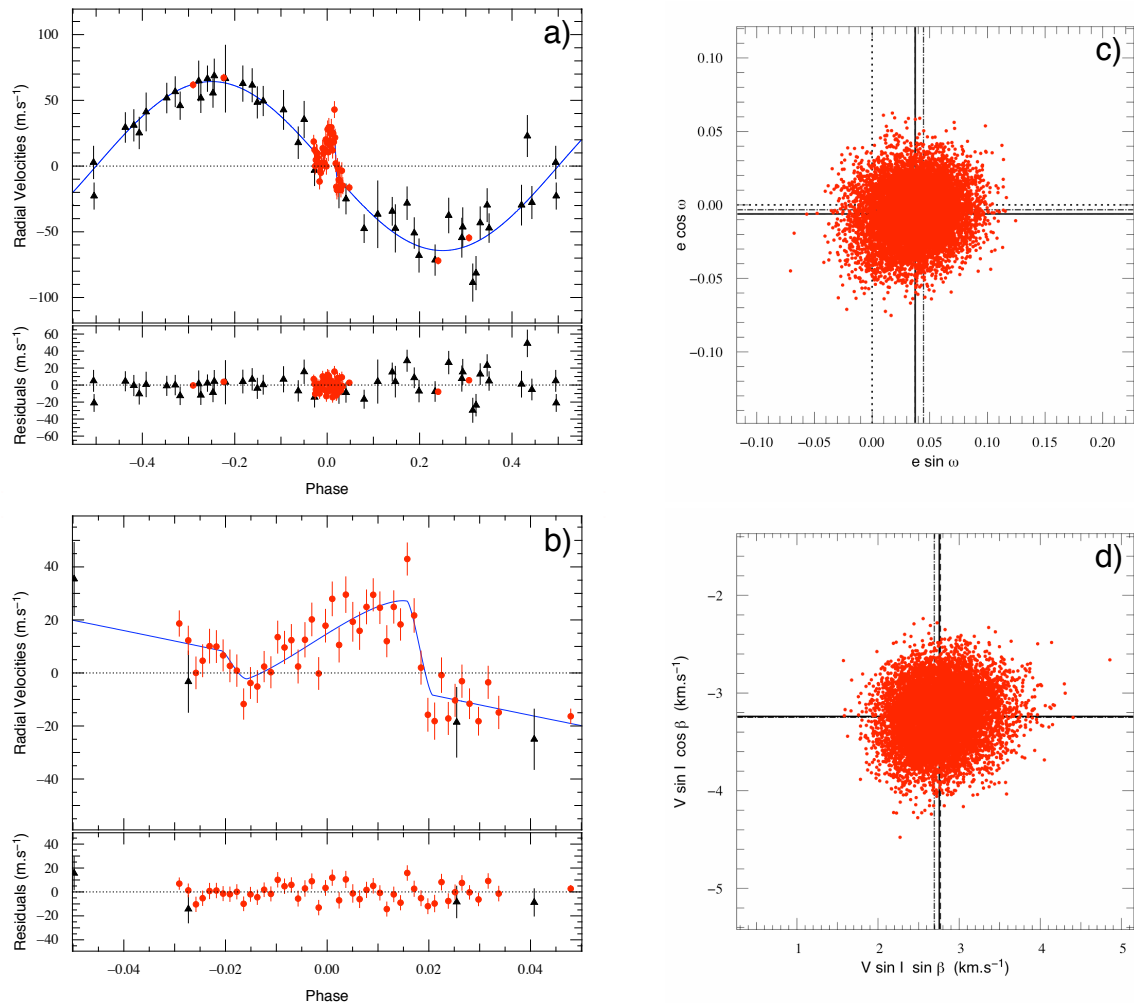
Fig. 5. Fit results for WASP-15b. *Nota Bene*: Legend similar to the legend in Fig.1.

Table 4. List of γ velocities for WASP-17's RV sets.

Instrument	Dataset	γ (m s^{-1})
CORALIE	*Rossiter-McLaughlin effect*	$-49500.80^{+2.62}_{-1.57}$
CORALIE	*orbital Doppler shift*	$-49513.67^{+0.46}_{-0.37}$
HARPS	*Rossiter-McLaughlin effect*	$-49490.59^{+2.72}_{-1.64}$
HARPS	*orbital Doppler shift*	$-49491.68^{+0.17}_{-0.17}$

a sequence of 42 spectra was acquired with a cadence of 630s during transit. They have a mean precision of 19.02 m s^{-1}. In addition to these and to data already published 12 CORALIE spectra and 15 HARPS spectra were obtained. All the spectroscopic data is presented in the appendices.

The photometry includes five timeseries of data in the WASP bandpass, and one *C2 Euler I* band transit (Anderson et al. 2010).

The model had to adjust up to 10 free floating parameters and 10 adjustment parameters (6 photometric normalisation factors and 4 radial velocity offsets) to 15 690 photometric data points and 124 spectroscopic points.

The RV was separated into four datasets fitted separately as detailed in Table 4. This was done to mitigate the possibility

that the RM effect was observed at a particular activity level for the star. Stellar activity adds an additional RV variation. For a set where this data is taken randomly over some time, one expects activity to act like a random scatter around a mean which would be the true γ velocity of the star in space. But for a sequence such as the RM effect, we expect only a slowly-varying radial-velocity bias caused by the activity level on the star on the night concerned. This analysis method is explained in Triaud et al. (2009) which showed an offset in γ velocities between different Rossiter-McLaughlin sequences of HD 189733 which can only be attributed to stellar variability. The large number of CORALIE and HARPS measurements outside transit and their large temporal span allowed us to separate RV sets for WASP-17 but not for the other targets. Table 4 shows the four values of γ. We remark a difference of 13 m s^{-1} for CORALIE, justifying our segmentation of the data.

Among the four computed chains, we select the circular priorless solution since our results show eccentricity is not significantly detected nor does the prior on $V \sin I$ appear to influence the end results.

The non significant eccentricity presented by Anderson et al. (2010) was not confirmed, so a circular orbit was adopted. We confine to within $e < 0.126$. Eccentricity affects the derived value of the stellar density, and thereby also affects the planet's radius measurement. Our circular solution suggests that WASP-
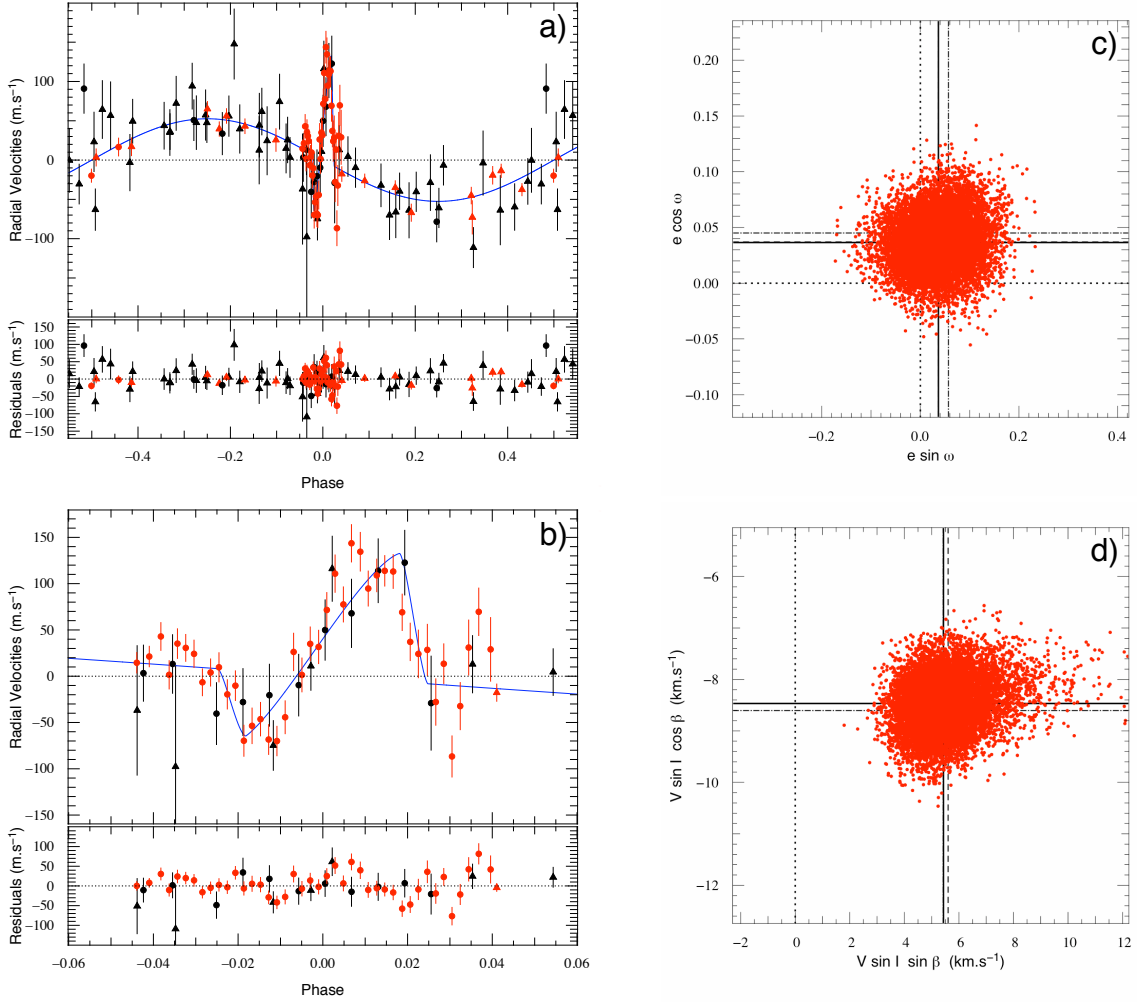
Fig. 6. Fit results for WASP-17b. On a) and b) black circles represent the RM effect taken with CORALIE, while black triangles picture the remaining CORALIE measurements; red dots show the HARPS RM data, red triangles are the remained HARPS points. *Nota Bene*: Legend similar to the legend in Fig.1.

17b's radius is $1.977^{+0.095}_{-0.079}\,R_{\rm J}$, making it the largest and least dense extrasolar planet discovered so far. We looked for an additional long term acceleration but found none: $|\dot{\gamma}| < 18\,{\rm m\,s^{-1}\,yr^{-1}}$.

The Rossiter-McLaughlin effect is well fitted. The residuals show some dispersion about the model during the HARPS sequence. At the end of the HARPS transit, the airmass attained high values which account for the larger error bars, the sparser sampling and higher dispersion. By comparison the CORALIE sequence appears better: its longer exposures blurred out short-term variability. Both $V\sin I$ and β are unambiguously detected. WASP-17b is on a severely misaligned orbit: $V\sin I = 10.14\,{\rm km\,s^{-1}}$ and $\beta = 147.3^{\circ\,+5.9}_{\ -5.5}$. Full results are displayed in Table 3.

4.6. WASP-18b

Soon after WASP-18b was confirmed by the spectrograph CORALIE, a Rossiter-McLaughlin effect was observed with HARPS. We obtained 19 measurements at a cadence of 630s on 2008 August 21. The mean photon noise for the transit sequence is $6.99\,{\rm m\,s^{-1}}$. Seeing and airmass improved during the sequence, increasing the S/N and decreasing the individual error bars. Additional data were also acquired out of transit. Hellier

et al. (2009) presented 9 RV measurements from CORALIE. 28 more have been taken and are presented in this paper. They span over three months. The total data timeseries spans close to 500 days. All RV measurements are presented in the journal of observations at the end of the paper.

Transit timing and geometry were secured by four photometric series: two SuperWASP seasons and two *C2 Euler* transits in *R* band, presented in Hellier et al. (2009).

The fitted data comprises 8593 photometric measurements and 60 radial velocities. Ten free parameters were used, with, in addition, four normalisation constants and two γ velocities.

Eccentricity is clearly detected, improving $\chi^2_{\rm reduced}$ from 5.67 ± 0.48 to 3.74 ± 0.39 (from 4.31 ± 0.46 to 2.00 ± 0.32 if we remove the RM effect from the calculation). We therefore exclude a circular solution.

Because the $V\sin I$ found in the priorless chain differed from the spectral analysis ($15.57^{+1.01}_{-0.69}$ instead of $11 \pm 1.5\,{\rm km\,s^{-1}}$), solutions using the prior are preferred. Therefore, the solution we favour is that of an eccentric orbit, with a prior on the $V\sin I$.

Results are presented in Table. 3, and the best fit is shown in Fig. 7. This Rossiter-McLaughlin effect is one of the largest so far measured, with an amplitude of nearly $185\,{\rm m\,s^{-1}}$. During the transit sequence $O - C = 15.35\,{\rm m\,s^{-1}}$ for a mean precision of
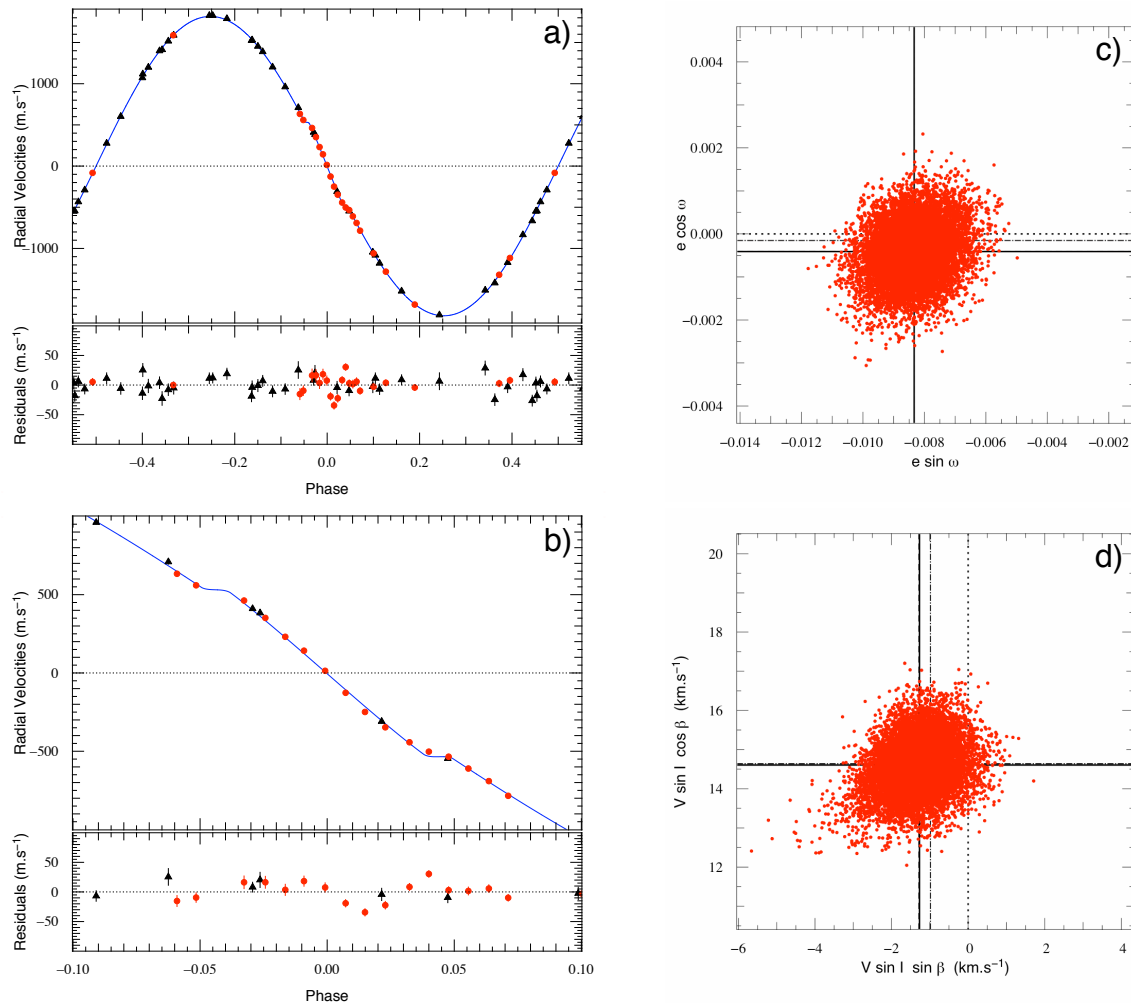
Fig. 7. Fit results for WASP-18b. *Nota Bene*: Legend similar to the legend in Fig.1.

6.95 m s^{-1}: the fit is poor; $\chi^2_{\mathrm{reduced}} = 3.74 \pm 0.39$. This is likely caused by a misfit of a symmetric Gaussian on a no longer symmetrical CCF[4]. We are in fact *resolving* the planet transit in front of the star like spots can be detected via Doppler tomography. This has recently been observed for HD 189733b, as a *Doppler shadow* (Cameron et al. 2010). The misfit causes an overestimation of $V \sin I$ thus confirming our decision to use the chain with a prior. The accuracy on the β parameter is not affected by the misfit since it is measured from the asymmetry of the Rossiter-McLaughlin effect. It is in essence estimated from the difference of time spent between the two hemisphere of the star.

Therefore all parameters can be trusted except the $V \sin I$, including the much sought after β angle. We find it to be consistent with zero within 1.5 σ: $\beta = -5.0°\,^{+3.1}_{-2.8}$. The precision on this angle is the best we measured. This is thanks to the brightness of the star, allowing precise measurements of a large amplitude effect. Any departure from the model is quickly penalised in χ^2 by the data. Similarly, eccentricity is detected above 9 σ with $e = 0.0084\,^{+0.0008}_{-0.0010}$ thanks to the large amplitude of the reflex motion. The spectroscopic coverage gives us the chance to

put some limits on an undetected long term radial velocity drift: $|\dot{\gamma}| < 43$ m s^{-1} yr^{-1}.

The other parameters are consistent with what has been published by Hellier et al. 2009 and are presented in Table 3.

5. Overall results

Our fits to the Rossiter-McLaughlin effect confirm the presence of planetary spectroscopic transit signatures in all six systems. While three of the six appear closely aligned, the other three exhibit highly-inclined, apparently retrograde orbits. The orbits of all six appear close to circular. Only the massive WASP-18b yields a significant detection of orbital eccentricity.

5.1. Orbital eccentricities

As observed in Gillon et al. (2009b), treating eccentricity as a free fitting parameter increases the error bars on other parameters; we are exploring a larger parameter space. One might argue that allowing eccentricity to float is necessary since no orbit is perfectly circular, therefore making an eccentric orbit the simplest model available. We argue against this for the simple reason that if statistically we cannot make a difference between an eccentric and a circular model then it shows that the eccentric

---

[4] this was noted in Triaud et al. (2009) in the case of HD 189733b and CoRoT-3b, but can also be seen on fits of CoRoT-2b (Bouchy et al. 2008), Hat-P-2b (Loeillet et al. 2008) and others.

model is not detected. Actually, the mere fact of letting eccentricity float biases the result towards a small non zero number, a bias which can be larger than the actual physical value (Lucy & Sweeney 1971). Hence letting eccentricity float when it is not detected is to allow values of parameter space for all parameters to be explored which do not need to be. This is why, unless χ^2 is significantly improved by adding two additional parameters to a circular model, we consider the former as preferable. To facilitate comparison, we also present the results of fits with floating eccentricity. These are given in the appendices; our preferred solutions are described in the text and in table 3.

Only for WASP-18b, have we detected some eccentricity in the orbit, thanks primarily to the high amplitude of the RV signal and the brightness of the target. The amount of RV data taken on WASP-18b is not really more than for the other targets. In addition to a high semi-amplitude, sampling is another key to fixing eccentricity properly. The lack of measured eccentricities on our other targets shows how difficult it is to measure a small eccentricity for these planets as long as no secondary transit is detected to constrain it. Spurious eccentricities tend to appear in fits to data sets where the radial velocities are not sampled uniformly around the orbit, and where the amplitude is small compared to the stellar and instrumental noise levels.

A good example is the case of WASP-17b for which the doubling of high precision RV points solely permitted us to place a tighter constraint compared to Anderson et al. (2010).

5.2. Fitting the Rossiter-McLaughlin effect

Our observations yielded results from which five sky-projected spin-orbit angles β have been determined with precision better than $15°$. Three of these angles appear to be retrograde: half our sample. Adding the two other stars from our original sample that have been published separately (WASP-6b and WASP-8b) we obtain 4 out of 8 angles being not just misaligned but also over $90°$.

The error bar on WASP-4b's β is large. A degeneracy appears when the impact parameter is close to 0 between $V \sin I$ and β. The estimate of the spin-orbit angle therefore relies on a good estimate of the stellar rotational velocity as well as with getting a stronger constraint on the impact parameter and on the shape of the Rossiter-McLaughlin effect.

When the planet is large compared to the parent star, or the star rotates rapidly, the cross-correlation function develops a significant asymmetry during transit. This happens because the spectral signature of the light blocked by the planet is partially resolved. Fitting a Gaussian to such a profile yields a velocity estimate that differs systematically from the velocity of the true light centroid. Winn et al. (2005), and later Triaud et al. (2009) and Hirano et al. (2010) showed how this effect can lead to over-estimation of $V \sin I$. Hirano et al. (2010) have developed an analytic method to compensate for this bias. Cameron et al. (2010) circumvent the problem altogether by modelling the CCF directly, decomposing the profile into a stellar rotation profile and a model of the light blocked by the planet.

Only one star in our sample suffers from this misfit: WASP-18b where easily we see that the value the fit issues for the $V \sin I$ is above the estimated value taken via spectral analysis. WASP-17b is the second fastest rotating star. If affected, it is not by much: the fitted $V \sin I$ is found within 1σ of the $v \sin I$.
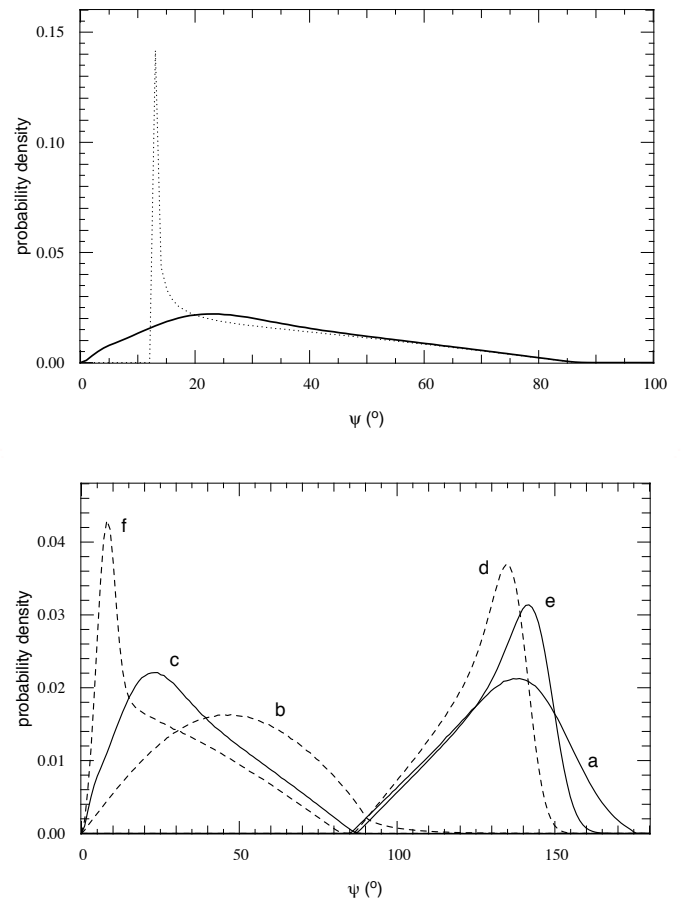
Fig. 8. *top* Smoothed histogram of the ψ distribution for WASP-5b. The dotted line is when errors on i and β are set to zero. The plain curve shows the same conversion from β to ψ but with all errors accounted for. *bottom*: 6 smoothed histograms of the distribution in ψ our six targets: a)-WASP-2b b)-WASP-4b c)-WASP-5b d)-WASP-15b e)-WASP-17b f)-WASP-18b. Bins are of $1°$.

As shown in Fabrycky & Winn (2009), we can get an idea of the real angle ψ from β by using the following equation, coming only from the geometry of the system:

$$\cos \psi = \cos I \cos i + \sin I \sin i \cos \beta \qquad (2)$$

where I is the inclination of the stellar spin axis and i the inclination of the planet's orbital axis to the line of sight.

Using the reasonable assumption that the stellar spin axis angle I is distributed isotropically, we computed the above equation using a simple Monte-Carlo simulation to draw a random uniform distribution in $\cos I$. We also inserted the error bars on i and β, using a Gaussian random number adjusted to the 1σ error bars printed in table 5. Fig. 8 shows the transformation from β to ψ for our targets, also illustrating the importance of including error bars in the calculation. We computed the lower ψ (at the 3σ limit) and found that in the stars we surveyed: WASP-17b is $> 90.2°$, therefore retrograde, while WASP-2b and WASP-15b are $> 88.3°$ and $> 89.1°$ but most likely retrograde.

Statistically we will fail to detect a Rossiter-McLaughlin effect (hence β and ψ) on stars nearly pole-on (with a low I). WASP-2b, with its small $V \sin I$ could be a close case. It could be one reason why its RM amplitude is so small (or stellar rotation so low). We observe that the spread in ψ is larger than for our other targets.

5.3. Correlations between parameters

We present a compilation of results from all known observations of the Rossiter-McLaughlin effect in transiting exoplanetary systems in Table 5. No clear correlation is evident between important planetary parameters such as radii, masses, eccentricities, orbital periods, β and $V \sin I$, except that planets with $M < 2\,M_J$ and $e > 0.1$ are rare among transiting systems (the only two are Neptunes around M dwarfs); this remark is independent from having a Rossiter-McLaughlin measurement or not. It is hard to see if this is really a result, or a bias due to observations (eg: transits harder to extract from the survey photometry, or to confirm via radial velocity), or a lack of precision during follow-up making eccentricity hard to detect with confidence. WASP-17b, for example, was previously thought to be the most eccentric transiting planet with $M < 2\,M_J$ but our analysis yields only an upper limit $e < 0.126$. Eccentricities with as great as $e = 0.1$ have been published for some planets with masses less that $2M_J$, none of these results are significant at more than the $\sim 2\,\sigma$ level.

The current ($M_p \sin i$, e) distribution in radial velocity does not show this result, but these masses are only minimum masses.

Amongst planets where eccentricity is firmly detected, four out of seven are misaligned. Some of the hot Jupiters appear to be in multiple systems but this appears unrelated to other parameters such as eccentricity or misalignment. Examples are: HD 189733 (Bakos et al. 2006), WASP-8 (Queloz et al., *submitted*), Hat-P-7 (Winn et al. 2009b) WASP-2, TrES-2 and TrES-4 (Daemgen et al. 2009).

6. Discussion

After a long sequence of closely-aligned planets (Fabrycky & Winn 2009), the sudden appearance of so many misaligned planets is somewhat surprising if not unpredicted. In a collapsing gas cloud, conservation of angular momentum will create a disc from which a star can form. Thus it is expected that star and disc rotate in the same direction with parallel spin axes. If planets form in and migrate through the disc, we can extend the idea that planets' orbital axes and stellar rotation axes ought to be parallel. Tides alone cannot make a planet retrograde (Hut 1981). Therefore it is expected that the creation of retrograde planets involves another body: planetary or stellar. Several papers (Fabrycky & Tremaine 2007; Nagasawa et al. 2008; Chatterjee et al. 2008; Jurić & Tremaine 2008; Bate et al. 2000, 2009) produce via various processes, orbits which are not coplanar with the host star's equator.

When combining the 26 RM effects that have been observed, we now see that eight planets are severely misaligned: XO-3b (Hébrard et al. 2008; Winn et al. 2009c) , HD 80606b (Moutou et al. 2009; Pont et al. 2009b; Winn et al. 2009a), WASP-14b (Johnson et al. 2009), Hat-P-7b (Winn et al. 2009b; Narita et al. 2009), WASP-8b (Queloz et al., *submitted*) and WASP-2b, WASP-15b and WASP17b. Of these eight, five have been found to be in retrograde orbits, four from our survey.

Three additional targets may be misaligned: Kepler-8b (Jenkins et al. 2010), CoRoT-1b (Pont et al. 2009a) and CoRoT-3b (Triaud et al. 2009). All three are around faint stars and fairly fast rotators making it hard to determine the angle. All β measurements have been plotted in Fig. 9a.

Because we only measure the sky-projection of the angle, the planets can in fact be in a variety of configurations. What is their real angle ψ distribution? We applied the method as in section 5.2 to all objects presented in table 5. Systems that appear aligned in β have a non negligible, additive probability that their
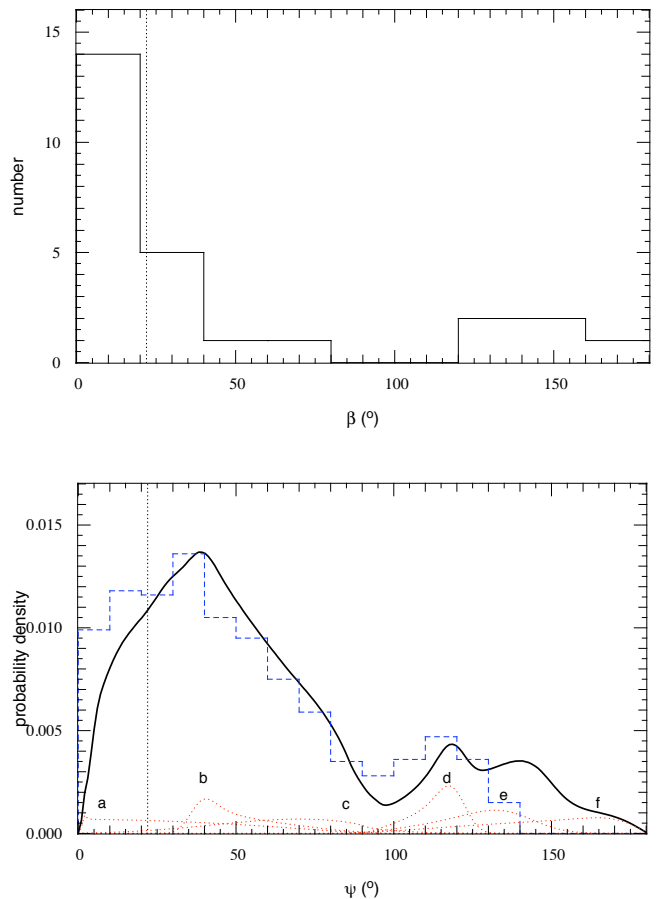
Fig. 9. *top*: Histogram of all the β measured, binned by 20°. *bottom*: The above histogram transformed into the real angle ψ in solid line and smoothed to bins of 1°. Red dotted curves show key individual objects in order to illustrate some of the features of the overall distribution. The blue dashed histogram is the reproduction of the theoretical histogram published by Fabrycky & Tremaine (2007) and solely plotted over. a)-HD 189733b b)-XO-3b c)-HD 80606b d)-WASP-8b e)-WASP-15b f)-Hat-P-7b. The black dotted line shows $\psi = 22°$. Above that, planets are considered misaligned.

real angle ψ is different from 0 as shown in Fig. 8a, notably due to $i < 90°$. Although only eight out of 26 objects are misaligned in β, when transforming β's in ψ by assuming an isotropic distribution of the angle I and accounting for errors in β and i, the overall ψ distribution indicates that the majority of planets are in fact misaligned[5]. Results are presented in Fig. 9b. We tested the robustness of this distribution by excluding the as-yet unrefereed objects; its shape was similar. Some key objects have been plotted on Fig. 9b to illustrate their influence on the overall distribution. When transforming β to ψ we found that 82.2 % of the probability density distribution is at $\psi > 22°$.

In order to further test this result we took the extreme case where all stellar axes I would be in a particular configuration. Namely, instead of having an isotropic distribution we resolved equation 2 for $\sin I = 1$, meaning we assume the hypothesis that all stellar axes are perpendicular to our line of sight. To come close to observations and to allow for some flexibility we took $\sin I = |1 \pm 0.05|$ (a variance smaller than current observed er-

---

[5] taking a criterion of misalignment as $\psi > 22°$, following the criterion calculated from the ψ distribution in the Solar System by Fabrycky & Winn (2009).
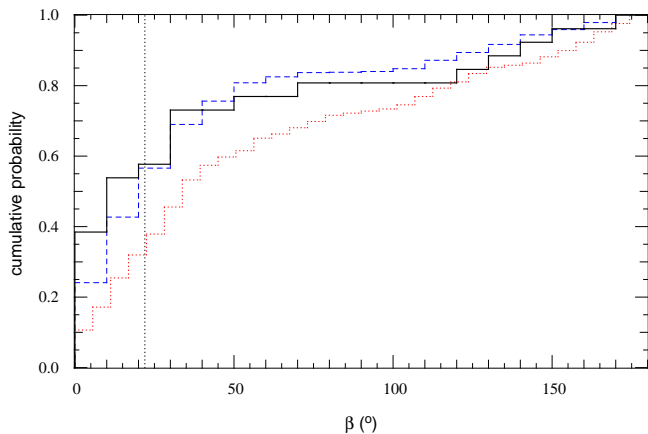
Fig. 10. Cumulative probability function for models by Fabrycky & Tremaine (2007) (blued dashed) and Nagasawa et al. (2008) (red dotted) converted from ψ to β, compared with current observations of β (plain black). The vertical black dotted line shows $\psi = 22°$. Above that, planets are considered misaligned.

ror bars). We find, as would be expected, a narrower distribution whose peak has moved closer to $\psi = 0°$, but 60.9 % of the distribution remains misaligned with $\psi > 22°$. This value is probably a lower estimate as there seems no reason why a planet with β misaligned should only be around stars with $I = 90°$. In fact this outcome shows that assuming $\sin I = 1$ is wrong, thus supporting our earlier assumption that stellar axes are isotropically distributed.

Aligned systems are no longer the norm, radically altering our view on how these hot Jupiters formed. We compared the ψ distributions obtained by the above mentioned theoretical papers and found one that reproduced well our results:

Fabrycky & Tremaine (2007) use the Kozai mechanism (Kozai 1962; Wu & Murray 2003) induced by an outer binary companion to the inner planet, to move the planet from the ice line where it is thought to form, to the inner stellar system. As the planet gets closer to the primary, tidal friction helps to break the Kozai cycles and finalise the planet's orbital parameters. Their equations are extracted from work by Eggleton & Kiseleva-Eggleton (2001). The resulting ψ distribution extends from 0° up to 150° away from the primary's rotation axis (see Fig. 9b). In this scenario, the planet can be created in a binary star system, or around a single star which acquired a companion through interactions in its cluster of origin (Pfahl & Muterspaugh 2006). Fabrycky & Tremaine (2007) following on a paper by Malmberg et al. (2007), also predict that in multi-planetary systems undergoing Kozai cycles thanks to a nearby star, the most massive planet would survive the resulting planet-planet scattering. Although Kozai cycles are usually associated with high eccentricities, we should not be surprised by the presence of so many misaligned planets on circular orbits. As simulated in the case of HD 80606b in Fabrycky & Tremaine (2007), the Kozai cycle has ended (is responsible the close proximity of the planet to the central star at periastron making precession dominated by general relativity rather than by the action of the third body). The planet appears now in a process of circularisation that will take ~ 0.7 Gyr, while its angle ψ remains almost constant.

The theoretical ψ distribution published by Fabrycky & Tremaine (2007) is shown superimposed on the ψ distribution inferred from observations in Fig. 9b. The histogram of available measurements gives a remarkably close match to the theoretical

prediction using only the Kozai mechanism and tidal friction. If the form of this distribution is borne out by future observations, we may then conclude that hot Jupiters are formed by this very mechanism without the need to invoke disc migration.

Nagasawa et al. (2008) model scattering processes between planets creating a pair where one planet is on a close orbit and the other around 40 to 100 AU which then drives Kozai cycles on the inner planet. They also use tidal friction with the star. These authors predict with orbits with a wide range distribution of inclinations and eccentricities which does not reproduce our observations as closely as Fabrycky & Tremaine (2007) do. All other authors fall short of the wide range of angles that we detect.

To further compare the observational data and theoretical predictions as well as for testing the robustness of our previous analysis, we also produce cumulative histograms in Fig. 10. We transformed histogram predictions from Fabrycky & Tremaine (2007) and Nagasawa et al. (2008) by taking their ψ and transforming them geometrically into observable β, with the assumption that I is isotropic. For a fixed ψ, we define an azimuthal angle α measured from a zero point where the star's north pole is tilted towards the observer. If we precess the star for $\alpha \in [0, 2\pi[$ we obtain β via a Monte Carlo simulation from solving:

$$\sin\beta \simeq \sin\psi \sin\alpha \tag{3}$$

using the conservative assumption that $i = 90°$ since these systems are transiting.

The observational data, β, has been overplotted. Observations and models by Fabrycky & Tremaine (2007) agree that about 55 % of planets should appear with $\beta < 30°$ (taken from the bin size). We clearly remark that predictions by Nagasawa et al. (2008) agree in range but not in the shape of distribution of observed β.

If the Kozai effect were found to be the dominant process leading to the creation of hot Jupiters, there is no reason why longer period planets should not have undergone similar cycles. The only difference would be that having greater periastron distances, tidal friction was less active. It would then be expected that lone Jupiters on large eccentric orbits be misaligned as well. HD 80606b would be part of that population. We could then have a *lone Jupiter* population of which *hot Jupiters* are a subset, and another planet population where Kozai migration did not act.

7. Conclusions

The observations reported here bring the total number of transiting planets with known sky-projected obliquities from 20 to 26. Among this enlarged sample, eight show significant projected spin-orbit misalignments; and of these eight, five show apparent retrograde motion. This projected angle β can be transformed statistically into the real spin-orbit angle ψ. Although 1/3 of planets have $\beta \neq 0°$, the distribution in ψ shows that 80% of hot Jupiters are misaligned. The angle range and shape of the overall ψ distribution appears consistent with the predictions of models by Fabrycky & Tremaine (2007) using the Kozai mechanism to make planets move inwards and tidal friction to reduce their semi-major axis and eventually, circularise them. This evidence is the strongest to suggest that processes others than type I or II migration (using exchange of angular momentum between a planet and a disc) are responsible for the creation of hot Jupiters. Type I or II migration alone cannot explain the observations. These results and conclusions should also be a call to account for environmental effects on planetary systems in planet formation simulations. These systems are not in isolation and interact with their neighbours.

Table 5. Comparative table of all Rossiter-McLaughlin effects published and parameters. Asterisks show claims of misalignments which remain to be confirmed.

Planet	R_p (R_J)	M_p (M_J)	e	P (day)	i (°)	β (°)	$V \sin I$ (km s^{-1})	references
HD 17156b	$1.23^{+0.17}_{-0.20}$	$3.09^{+0.22}_{-0.17}$	$0.6719^{+0.0052}_{-0.0063}$	$21.21747^{+0.00070}_{-0.00067}$	$85.4^{+1.9}_{-1.2}$	-9.4 ± 9.3	6.3 ± 1.1	Cochran et al. (2008); Gillon et al. (2008)
HD 80606b	0.9 ± 0.1	4.0 ± 0.3	0.934 ± 0.003	111.436 ± 0.003	89.6 ± 0.4	-53^{+21}_{-34}	2.2	Moutou et al. (2009); Winn et al. (2009a)
HD 147506b	$0.951^{+0.039}_{-0.053}$	8.62 ± 0.1	$0.5163^{+0.0025}_{-0.0023}$	5.63341 ± 0.00013	$90.00^{+0.85}_{-0.93}$	$-0.2^{+12.2}_{-12.5}$	$22.9^{+1.1}_{-1.2}$	Loeillet et al. (2008)
HD 149026b	0.718 ± 0.065	0.352 ± 0.025	0	$2.87618^{+0.00033}_{-0.00018}$	86.1 ± 1.4	12 ± 15	$6.2^{+2.1}_{-0.6}$	Wolf et al. (2007)
HD 189733b	$1.178^{+0.016}_{-0.023}$	1.138 ± 0.022	$0.0041^{+0.0025}_{-0.0020}$	$2.218573112^{+0.000000036}_{-0.000000076}$	$85.51^{+0.10}_{-0.05}$	$0.85^{+0.28}_{-0.32}$	$3.316^{+0.017}_{-0.067}$	Triaud et al. (2009)
HD 209458b	1.355 ± 0.002	0.657 ± 0.006	0.0147 ± 0.0053	$3.52474859 \pm 0.00000038$	86.55 ± 0.03	4.4 ± 1.4	4.70 ± 0.16	Winn et al. (2005); Knutson et al. (2007)
XO-3b	1.5 ± 0.2	12.5 ± 1.9	0.2884 ± 0.0035	3.19161 ± 0.00014	82.5 ± 1.5	-37.3 ± 3.7	18.31 ± 1.3	Hébrard et al. (2008); Winn et al. (2009c)
HAT-P-1b	1.225 ± 0.059	0.524 ± 0.031	0	4.4652934 ± 0.0000093	86.28 ± 0.20	-3.7 ± 2.1	3.75 ± 0.58	Johnson et al. (2008)
HAT-P-7b	$1.363^{+0.195}_{-0.087}$	$1.776^{+0.077}_{-0.049}$	0	2.2047304 ± 0.0000024	$80.8^{+2.8}_{-1.2}$	-182.5 ± 9.4	$4.9^{+1.2}_{-0.9}$	Pál et al. (2008); Winn et al. (2009b); Narita et al. (2009)
TrES-1b	1.081 ± 0.029	0.61 ± 0.06	0	3.0300722 ± 0.0000002	88.4 ± 0.3	-30 ± 21	1.3 ± 0.3	Narita et al. (2007)
TrES-2b	$1.220^{+0.045}_{-0.042}$	1.198 ± 0.053	0	2.470621 ± 0.00017	83.62 ± 0.14	9 ± 12	1.0 ± 0.6	Winn et al. (2008); Daemgen et al. (2009)
TrES-4b	1.674 ± 0.094	0.84 ± 0.10	0	3.553945 ± 0.000075	82.81 ± 0.33	-7.3 ± 4.6	8.3 ± 1.1	Mandushev et al. (2007); Narita et al. (2010)
CoRoT-1b*	1.49 ± 0.08	1.03 ± 0.12	0	1.5089557 ± 0.0000064	85.1 ± 0.5	77 ± 11	5.2 ± 1.0	Barge et al. (2008); Pont et al. (2009a)
CoRoT-2b	1.465 ± 0.029	3.31 ± 0.16	0	1.7429964 ± 0.0000017	87.84 ± 0.10	-7.1 ± 5.0	$11.46^{+0.29}_{-0.44}$	Alonso et al. (2008); Bouchy et al. (2008)
CoRoT-3b*	$0.9934^{+0.0058}_{-0.0058}$	$21.23^{+0.82}_{-0.59}$	$0.008^{+0.015}_{-0.005}$	$4.2567994^{+0.0000039}_{-0.0000031}$	$86.10^{+0.73}_{-0.52}$	$37.6^{+10.0}_{-22.3}$	$35.8^{+8.2}_{-8.3}$	Triaud et al. (2009)
Kepler-8b*	$1.419^{+0.056}_{-0.058}$	$0.60^{+0.13}_{-0.19}$	0	$3.52254^{+0.00007}_{-0.00005}$	84.07 ± 0.33	26.9 ± 4.6	10.5 ± 0.7	Jenkins et al. (2010)
WASP-2b	$1.077^{+0.055}_{-0.058}$	$0.866^{+0.076}_{-0.084}$	0	$2.1522254^{+0.0000015}_{-0.0000014}$	$84.73^{+0.18}_{-0.19}$	153^{+11}_{-15}	$0.99^{+0.27}_{-0.32}$	This paper
WASP-3b	$1.29^{+0.05}_{-0.07}$	$1.76^{+0.06}_{-0.14}$	0	1.846835 ± 0.000002	$84.93^{+1.32}_{-0.80}$	-14 ± 9	19.6 ± 2.2	Pollacco et al. (2008); Simpson et al. (2009)
WASP-4b	$1.341^{+0.023}_{-0.029}$	$1.250^{+0.050}_{-0.085}$	0	$1.3382299^{+0.0000023}_{-0.0000021}$	$89.47^{+0.51}_{-0.24}$	-4^{+43}_{-34}	$2.14^{+0.38}_{-0.35}$	This paper
WASP-5b	$1.14^{+0.10}_{-0.04}$	$1.555^{+0.081}_{-0.081}$	0	$1.6284229^{+0.0000044}_{-0.0000032}$	$86.2^{+0.8}_{-1.7}$	$-12.4^{+11.9}_{-8.2}$	$3.24^{+0.35}_{-0.35}$	This paper
WASP-6b	$1.224^{+0.051}_{-0.052}$	$0.503^{+0.019}_{-0.038}$	0	$3.3610060^{+0.0000022}_{-0.0000035}$	$88.47^{+0.65}_{-0.47}$	11^{+14}_{-18}	$1.6^{+0.27}_{-0.17}$	Gillon et al. (2009a)
WASP-8b	1.02 ± 0.05	2.20 ± 0.06	0.311 ± 0.002	8.15871578 ± 0.00001	$88.52^{+0.42}_{-0.25}$	120 ± 4	1.62 ± 0.08	Queloz 2009
WASP-14b	$1.281^{+0.075}_{-0.082}$	7.34 ± 0.51	0.0903 ± 0.0027	2.23752 ± 0.000010	$84.32^{+0.67}_{-0.72}$	33.1 ± 7.4	2.89 ± 0.57	Joshi et al. (2009); Johnson et al. (2009)
WASP-15b	$1.379^{+0.087}_{-0.082}$	$0.551^{+0.041}_{-0.040}$	0	$3.752100^{+0.000009}_{-0.000009}$	$85.96^{+0.35}_{-0.35}$	$139.6^{+5.2}_{-4.3}$	$4.27^{+0.26}_{-0.36}$	This paper
WASP-17b	$1.977^{+0.085}_{-0.095}$	$0.453^{+0.034}_{-0.042}$	0	$3.7354332^{+0.0000080}_{-0.0000091}$	$86.71^{+0.38}_{-0.31}$	$147.3^{+5.9}_{-5.5}$	$10.14^{+0.58}_{-0.58}$	This paper
WASP-18b	$1.228^{+0.067}_{-0.036}$	$10.11^{+0.22}_{-0.23}$	$0.0084^{+0.0008}_{-0.0010}$	$0.94145298^{+0.00000092}_{-0.00000074}$	$81.6^{+1.0}_{-1.5}$	$-5.0^{+3.1}_{-2.8}$	$14.67^{+0.81}_{-0.57}$	This paper

We are seeing the coming of a new diversity in planetary parameters, coming after large diversities in mass, period, eccentricity and radius. The variety of angles β, transformed into ψ, is an indication of the physical processes that happened before, during and after planet formation. Once again the measurement of a new observable has brought a large variety of values reflecting how rich nature is.

As more transiting systems are discovered in wide-field surveys, and follow-up observations of the kind reported here are made, the statistical picture that is beginning to emerge will become clearer.

References

Alonso, R., Auvergne, M., Baglin, A., et al. 2008, A&A, 482, L21
Anderson, D. R., Gillon, M., Hellier, C., et al. 2008, MNRAS, 387, L4
Anderson, D. R., Hellier, C., Gillon, M., et al. 2010, ApJ, 709, 159
Bakos, G. Á., Pál, A., Latham, D. W., Noyes, R. W., & Stefanik, R. P. 2006, ApJ, 641, L57
Baranne, A., Queloz, D., Mayor, M., et al. 1996, A&A, 119, 373
Barge, P., Baglin, A., Auvergne, M., et al. 2008, A&A, 482, L17
Barker, A. J. & Ogilvie, G. I. 2009, MNRAS, 481
Bate, M. R., Bonnell, I. A., Clarke, C. J., et al. 2000, MNRAS, 317, 773
Bate, M. R., Lodato, G., & Pringle, J. E. 2009, eprint arXiv, 0909, 4255
Bouchy, F., Queloz, D., Deleuil, M., et al. 2008, A&A, 482, L25
Cameron, A. C., Bouchy, F., Hébrard, G., et al. 2007, MNRAS, 375, 951
Cameron, A. C., Bruce, V. A., Miller, G. R. M., Triaud, A. H. M. J., & Queloz, D. 2010, MNRAS, 180
Castelli, F., Gratton, R. G., & Kurucz, R. L. 1997, A&A, 318, 841
Charbonneau, D., Brown, T. M., Latham, D. W., & Mayor, M. 2000, ApJ, 529, L45
Charbonneau, D., Winn, J. N., Everett, M. E., et al. 2007, ApJ, 658, 1322
Chatterjee, S., Ford, E. B., Matsumura, S., & Rasio, F. A. 2008, ApJ, 686, 580
Claret, A. 2000, A&A, 363, 1081
Cochran, W. D., Redfield, S., Endl, M., & Cochran, A. L. 2008, ApJ, 683, L59
Daemgen, S., Hormuth, F., Brandner, W., et al. 2009, A&A, 498, 567
Eggleton, P. P. & Kiseleva-Eggleton, L. 2001, ApJ, 562, 1012
Fabrycky, D. & Tremaine, S. 2007, ApJ, 669, 1298
Fabrycky, D. C. & Winn, J. N. 2009, ApJ, 696, 1230
Gaudi, B. S. & Winn, J. N. 2007, ApJ, 655, 550
Gillon, M., Anderson, D. R., Triaud, A. H. M. J., et al. 2009a, A&A, 501, 785
Gillon, M., Demory, B. O., Triaud, A. H. M. J., et al. 2009b, eprint arXiv, 0905, 4571
Gillon, M., Smalley, B., Hebb, L., et al. 2009c, A&A, 496, 259
Gillon, M., Triaud, A. H. M. J., Mayor, M., et al. 2008, A&A, 485, 871
Giménez, A. 2006, ApJ, 650, 408
Goldreich, P. & Tremaine, S. 1980, ApJ, 241, 425
Gray, D. F. 2008, The Observation and Analysis of Stellar Photospheres
Hébrard, G., Bouchy, F., Pont, F., et al. 2008, A&A, 488, 763
Hellier, C., Anderson, D. R., Cameron, A. C., et al. 2009, Nature, 460, 1098
Henry, G. W., Marcy, G. W., Butler, R. P., & Vogt, S. S. 2000, ApJ, 529, L41
Hilditch, R. W. 2001, An Introduction to Close Binary Stars
Hirano, T., Suto, Y., Taruya, A., et al. 2010, ApJ, 709, 458
Hosokawa, Y. 1953, PASJ, 5, 88
Hrudková, M., Skillen, I., Benn, C., et al. 2009, Transiting Planets, 253, 446
Hut, P. 1981, A&A, 99, 126
Jenkins, J. M., Borucki, W. J., Koch, D. G., et al. 2010, eprint arXiv, 1001, 416
Johnson, J. A., Winn, J. N., Albrecht, S., et al. 2009, PASP, 121, 1104
Johnson, J. A., Winn, J. N., Narita, N., et al. 2008, ApJ, 686, 649
Joshi, Y. C., Pollacco, D., Cameron, A. C., et al. 2009, MNRAS, 392, 1532
Jurić, M. & Tremaine, S. 2008, ApJ, 686, 603
Knutson, H. A., Charbonneau, D., Noyes, R. W., Brown, T. M., & Gilliland, R. L. 2007, ApJ, 655, 564
Kozai, Y. 1962, AJ, 67, 591
Lin, D. N. C., Bodenheimer, P., & Richardson, D. C. 1996, Nature, 380, 606
Loeillet, B., Shporer, A., Bouchy, F., et al. 2008, A&A, 481, 529
Lovis, C. & Pepe, F. 2007, A&A, 468, 1115
Lucy, L. B. & Sweeney, M. A. 1971, AJ, 76, 544
Malmberg, D., Davies, M. B., & Chambers, J. E. 2007, MNRAS, 377, L1
Mandel, K. & Agol, E. 2002, ApJ, 580, L171
Mandushev, G., O'Donovan, F. T., Charbonneau, D., et al. 2007, ApJ, 667, L195
Mayor, M., Bonfils, X., Forveille, T., et al. 2009, A&A, 507, 487
Mayor, M., Pepe, F., Queloz, D., et al. 2003, The Messenger (ISSN0722-6691), 114, 20
Mayor, M. & Queloz, D. 1995, Nature, 378, 355
McLaughlin, D. B. 1924, ApJ, 60, 22
Moutou, C., Hébrard, G., Bouchy, F., et al. 2009, A&A, 498, L5
Nagasawa, M., Ida, S., & Bessho, T. 2008, ApJ, 678, 498
Narita, N., Enya, K., Sato, B., et al. 2007, PASJ, 59, 763
Narita, N., Sato, B., Hirano, T., & Tamura, M. 2009, PASJ, 61, L35
Narita, N., Sato, B., Hirano, T., et al. 2010, eprint arXiv, 1003, 2268
Ohta, Y., Taruya, A., & Suto, Y. 2005, ApJ, 622, 1118
Pál, A., Bakos, G. Á., Torres, G., et al. 2008, ApJ, 680, 1450
Pepe, F., Mayor, M., Galland, F., et al. 2002, A&A, 388, 632
Pfahl, E. & Muterspaugh, M. 2006, ApJ, 652, 1694
Pollacco, D., Skillen, I., Cameron, A. C., et al. 2008, MNRAS, 385, 1576
Pollacco, D. L., Skillen, I., Cameron, A. C., et al. 2006, PASP, 118, 1407
Pont, F., Endl, M., Cochran, W. D., et al. 2009a, arXiv, astro-ph.EP
Pont, F., Hébrard, G., Irwin, J. M., et al. 2009b, A&A, 502, 695
Queloz, D., Eggenberger, A., Mayor, M., et al. 2000, A&A, 359, L13
Rasio, F. A. & Ford, E. B. 1996, Science, 274, 954
Rossiter, R. A. 1924, ApJ, 60, 15
Simpson, E. K., Pollacco, D., Hebrard, G., et al. 2009, arXiv, astro-ph.EP
Smalley, B., Smith, K. C., & Dworetsky, M. M. 2001, UCLSYN Userguide
Smith, K. C. 1992, PhD Thesis, University of London
Tegmark, M., Strauss, M. A., Blanton, M. R., et al. 2004, PhRvD, 69, 103501
Triaud, A. H. M. J., Queloz, D., Bouchy, F., et al. 2009, eprint arXiv, 0907, 2956
West, R. G., Anderson, D. R., Gillon, M., et al. 2009, AJ, 137, 4834
Wilson, D. M., Gillon, M., Hellier, C., et al. 2008, ApJ, 675, L113
Winn, J. N., Howard, A. W., Johnson, J. A., et al. 2009a, ApJ, 703, 2091
Winn, J. N., Johnson, J. A., Albrecht, S., et al. 2009b, ApJ, 703, L99
Winn, J. N., Johnson, J. A., Fabrycky, D., et al. 2009c, ApJ, 700, 302
Winn, J. N., Johnson, J. A., Narita, N., et al. 2008, ApJ, 682, 1283
Winn, J. N., Noyes, R. W., Holman, M. J., et al. 2005, ApJ, 631, 1215
Wolf, A. S., Laughlin, G., Henry, G. W., et al. 2007, ApJ, 667, 549
Wu, Y. & Murray, N. 2003, ApJ, 589, 605

Appendix A: Comparative tables for each star

Here, for transparency, are the tables recording the results from the various fits that were done for each star, which, par comparing them, led to the choice of our solutions.

Appendix B: Journal of Observations

The Radial-Velocity data extracted by fitting a Gaussian function on a Cross-Correlation Function resulting from comparing the spectra with a mask corresponding to its spectral type. The data is presented per instrument and separated in various datasets: overall Doppler shift and Rossiter-McLaughlin effect, as was done for the fits. Within each dataset, it is presented chronologically.

Table B.1. RV data for WASP-2b.

bjd (- 2 450 000)	RV (km s^{-1})	σ_{RV} (km s^{-1})	t_{exp} (s)
SOPHIE	*orbital Doppler shift*		
3982.3786	-27.711	0.012	2500
3982.4962	-27.736	0.013	2500
3991.3817	-27.780	0.011	1200
3991.5102	-27.812	0.011	1200
3996.3529	-28.037	0.011	1200
3996.4301	-28.020	0.012	1200
3997.3824	-27.723	0.012	1500
3998.3415	-27.987	0.011	1200
CORALIE	*orbital Doppler shift*		
4764.504689	-27.85981	0.01932	1801
4765.509206	-27.65742	0.02299	1801
4766.508375	-27.84650	0.01380	1801
4769.512698	-27.78332	0.01319	1801
4770.508244	-27.70918	0.01711	1801
4771.509646	-27.82787	0.01391	1801
4772.519878	-27.64359	0.01484	1801
4773.513595	-27.88050	0.01411	1801
4774.515784	-27.61010	0.01413	1801
4775.512417	-27.90960	0.01485	1801
4776.512326	-27.61153	0.02040	1801
5001.827721	-27.81832	0.01152	1801
5013.750160	-27.71932	0.01163	1801
5037.699667	-27.85913	0.01200	1801
5038.721568	-27.68417	0.00961	1801
5039.689751	-27.79590	0.01101	1801
5041.718024	-27.72765	0.01018	1801
5042.650566	-27.84181	0.00947	1801
5092.543315	-27.70924	0.01325	1801
5097.558717	-27.68199	0.01203	1801
HARPS	*Rossiter-McLaughlin effect*		
4754.528495	-27.70390	0.00702	900
4754.620408	-27.66549	0.00477	900
4755.490831	-27.71635	0.00649	400
4755.495101	-27.72204	0.00675	400
4755.500251	-27.72739	0.00458	300
4755.505239	-27.72374	0.00441	300
4755.509984	-27.72192	0.00491	400
4755.515331	-27.72547	0.00650	400
4755.520226	-27.72620	0.00469	400
4755.525087	-27.72943	0.00461	400
4755.530133	-27.74799	0.00516	400
4755.535179	-27.73390	0.00495	400
4755.540074	-27.73202	0.00498	400
4755.545178	-27.73969	0.00502	400
4755.550166	-27.72911	0.00498	400
4755.555073	-27.72841	0.00500	400
4755.560015	-27.74669	0.00595	400
4755.565061	-27.74516	0.00671	400
4755.570164	-27.73728	0.00604	400
4755.575164	-27.74225	0.00656	400
4755.580025	-27.74699	0.00679	400
4755.585070	-27.75745	0.00643	400
4755.590070	-27.74940	0.00709	400
4755.595197	-27.76458	0.00730	400
4755.602187	-27.77178	0.00522	600
4755.609420	-27.75318	0.00492	600
4755.616885	-27.75791	0.00581	600
4755.624130	-27.77039	0.00506	600
4756.503729	-27.79724	0.00242	900
4756.556086	-27.77834	0.00285	900

Table B.2. RV data for WASP-4b.

bjd (- 2 450 000)	RV (km s^{-1})	σ_{RV} (km s^{-1})	t_{exp} (s)
CORALIE	*orbital Doppler shift*		
4359.710824	57.57468	0.02053	1801
4362.631217	57.80604	0.02094	1801
4364.652602	57.68875	0.02460	1801
4365.736906	57.95170	0.01778	1801
4372.757994	57.59277	0.01652	1801
4376.688827	57.64569	0.01605	1801
4378.668871	57.79988	0.01458	1801
4379.736306	57.52086	0.01624	1801
4380.610348	57.78459	0.01437	1801
4382.790257	57.87592	0.02015	1801
4383.552773	57.50732	0.01570	1801
4387.619048	57.51081	0.01611	1801
4408.661101	57.79088	0.01875	1801
4409.519323	57.84236	0.02407	1801
4720.589143	57.73974	0.02532	1801
4722.674920	57.90628	0.01727	1801
4725.569004	58.00982	0.02329	1801
4729.588760	57.98945	0.01967	1801
4730.646040	57.82448	0.01753	1801
4760.593166	57.84475	0.01749	1801
4761.639625	57.99209	0.01691	1801
4762.654627	57.70943	0.01785	1801
4763.603116	57.52516	0.01753	1801
4763.725804	57.48750	0.02455	1801
HARPS	*Rossiter-McLaughlin effect*		
4747.809113	57.61982	0.00597	900
4748.501785	57.94526	0.00544	900
4748.552731	57.89782	0.00623	600
4748.560173	57.88884	0.00616	600
4748.567684	57.88212	0.00639	600
4748.575207	57.87224	0.00661	600
4748.582857	57.87643	0.00716	600
4748.590241	57.83952	0.00705	600
4748.597752	57.84293	0.00710	600
4748.605332	57.83795	0.00672	600
4748.612716	57.86116	0.00730	600
4748.620308	57.85916	0.00703	600
4748.627958	57.84646	0.00747	600
4748.635273	57.81970	0.00725	600
4748.642865	57.81142	0.00671	600
4748.650446	57.79059	0.00649	600
4748.657957	57.76719	0.00594	600
4748.665329	57.75065	0.00574	600
4748.672910	57.73640	0.00618	600
4748.680421	57.73107	0.00673	600
4748.688001	57.71750	0.00640	600
4748.695374	57.74694	0.00602	600
4748.703024	57.72254	0.00621	600
4748.710546	57.71510	0.00564	600
4748.718069	57.71593	0.00573	600
4748.725511	57.69356	0.00562	600
4748.733034	57.68893	0.00570	600
4748.740545	57.70283	0.00599	600
4748.748056	57.69677	0.00603	600
4748.755579	57.67217	0.00624	600
4748.763090	57.68511	0.00652	600
4750.744196	57.89058	0.00405	1800

Table B.3. RV data for WASP-5b.

bjd (- 2 450 000)	RV (km s^{-1})	σ_{RV} (km s^{-1})	t_{exp} (s)
CORALIE	*orbital Doppler shift*		
4359.614570	19.78859	0.01785	1801
4362.654785	19.94934	0.01630	1801
4364.676219	19.76409	0.02288	1801
4365.682733	20.20817	0.01378	1801
4372.781658	19.75922	0.01459	1801
4374.817984	20.01631	0.04516	1801
4376.714797	20.26098	0.01558	1801
4377.762440	19.75519	0.01445	1801
4379.627523	19.91862	0.01587	1801
4380.682557	19.84080	0.01142	1801
4387.644986	19.82288	0.01649	1801
4720.835375	20.05679	0.01816	1801
4724.603499	19.73117	0.01661	1801
4732.745208	19.74646	0.01812	1802
4733.686048	20.16201	0.01556	1801
4734.694930	19.99692	0.01726	1801
HARPS	*Rossiter-McLaughlin effect*		
4749.722428	20.29554	0.00334	1200
4750.766740	19.83105	0.00361	1800
4753.696462	19.79468	0.00391	1800
4754.773661	20.25200	0.00338	1800
4756.491182	20.18379	0.00363	900
4756.570483	20.11309	0.00456	600
4756.578469	20.11813	0.00483	600
4756.586466	20.09061	0.00527	600
4756.594846	20.08995	0.00551	600
4756.602762	20.08266	0.00497	600
4756.610747	20.07852	0.00478	600
4756.618814	20.06709	0.00485	600
4756.626904	20.05854	0.00512	600
4756.635121	20.06323	0.00462	600
4756.643107	20.06533	0.00456	600
4756.651173	20.06765	0.00439	600
4756.659090	20.05028	0.00496	600
4756.667399	20.02693	0.00544	600
4756.675223	20.01679	0.00543	600
4756.683440	19.98896	0.00543	600
4756.691345	19.97164	0.00657	600
4756.699261	19.95174	0.00564	600
4756.707640	19.95588	0.00544	600
4756.715788	19.95272	0.00518	600
4756.723530	19.94652	0.00542	600
4756.731748	19.94944	0.00645	600
4756.739965	19.94136	0.00637	600
4756.747869	19.93104	0.00559	600
4756.755936	19.93294	0.00689	600
4756.764084	19.92913	0.00640	600
4756.772069	19.90027	0.00690	600
4756.780067	19.90065	0.00678	600
4756.788295	19.88500	0.00731	600

Table B.4. RV data for WASP-15b.

bjd (- 2 450 000)	RV (km s^{-1})	σ_{RV} (km s^{-1})	t_{exp} (s)
CORALIE	*orbital Doppler shift*		
4531.814597	-2.26646	0.01478	1801
4532.722143	-2.35660	0.01795	1801
4533.746849	-2.33893	0.01512	1801
4534.877800	-2.24444	0.01510	1801
4535.734111	-2.27377	0.01376	1801
4536.666620	-2.37725	0.01261	1801
4537.780541	-2.33201	0.00992	1801
4538.745908	-2.25366	0.01081	1801
4556.794821	-2.27983	0.01122	1801
4557.748799	-2.24646	0.01339	1801
4558.733390	-2.35678	0.01057	1801
4559.747899	-2.35637	0.01085	1801
4560.615839	-2.27820	0.01189	1801
4589.658970	-2.39063	0.01261	1801
4591.635494	-2.26077	0.01184	1801
4655.468928	-2.25970	0.01109	1801
4656.516477	-2.34362	0.01056	1801
4657.613442	-2.28634	0.01558	1801
4662.520488	-2.24271	0.00960	1801
4663.587927	-2.32780	0.01314	1801
4664.593196	-2.35564	0.01468	1801
4834.855119	-2.25263	0.01138	1801
4835.854025	-2.29142	0.01198	1801
4840.827799	-2.34679	0.01314	1801
4859.843943	-2.35241	0.01213	1801
4881.821230	-2.36013	0.01160	1801
4882.776419	-2.33694	0.01217	1801
4884.763791	-2.31248	0.01155	1801
4889.711779	-2.36367	0.01480	1801
4890.844581	-2.28402	0.01194	1801
4891.761831	-2.24770	0.01257	1801
4939.677986	-2.26803	0.01438	1801
4943.706114	-2.26328	0.01040	1801
4945.776216	-2.38071	0.01152	1801
4947.626310	-2.25749	0.01094	1801
4948.804753	-2.33422	0.01136	1801
4949.833876	-2.39783	0.01413	1801
4971.575204	-2.34588	0.02533	1801
4973.614431	-2.25744	0.01122	1801
4975.565332	-2.33745	0.01238	1801
4983.719667	-2.33892	0.01251	1801
4995.532602	-2.30644	0.01228	1801
4996.512783	-2.24056	0.01272	1801
5011.611762	-2.24270	0.02538	1801
HARPS	*Rossiter-McLaughlin effect*		
4947.563543	-2.23262	0.00254	1800
4947.812040	-2.22718	0.00256	1800
4948.542784	-2.27576	0.00475	600
4948.549428	-2.28213	0.00535	500
4948.555099	-2.29438	0.00598	400
4948.560029	-2.28980	0.00601	400
4948.565111	-2.28430	0.00636	400
4948.570192	-2.28446	0.00600	400
4948.575134	-2.28779	0.00585	400
4948.580168	-2.29174	0.00598	400
4948.585261	-2.29353	0.00592	400
4948.590284	-2.30613	0.00571	400
4948.595319	-2.29820	0.00582	400
4948.600400	-2.29954	0.00600	400
4948.605435	-2.29201	0.00570	400
4948.610423	-2.29414	0.00585	400
4948.615423	-2.28089	0.00602	400
4948.620458	-2.28480	0.00607	400
4948.625539	-2.28205	0.00590	400
4948.630481	-2.29198	0.00621	400
4948.635562	-2.28189	0.00646	400
4948.640609	-2.27422	0.00615	400
4948.645690	-2.29462	0.00599	400
4948.650713	-2.27658	0.00615	400
4948.655701	-2.26646	0.00636	400
4948.660747	-2.28384	0.00643	400

Table B.5. RV data for WASP-17b.

bjd (- 2 450 000)	RV (km s^{-1})	σ_{RV} (km s^{-1})	t_{exp} (s)
CORALIE	*orbital Doppler shift*		
4329.603717	-49.45704	0.04276	1801
4360.486284	-49.36606	0.04444	1801
4362.497988	-49.51747	0.04074	1801
4364.487972	-49.48913	0.04321	1801
4367.488333	-49.44153	0.03428	1801
4558.883883	-49.49882	0.03107	1801
4559.770757	-49.57983	0.03246	1801
4560.731432	-49.57336	0.02950	1801
4588.779923	-49.48810	0.02888	1801
4591.777793	-49.46606	0.03401	1801
4622.691662	-49.39756	0.03508	1801
4624.636716	-49.44937	0.03672	1801
4651.619514	-49.45639	0.03187	1801
4659.524574	-49.46930	0.04045	1801
4664.642452	-49.54237	0.03533	1801
4665.659284	-49.49053	0.03768	1801
4682.582361	-49.50072	0.03086	1801
4684.626422	-49.51688	0.03572	1801
4685.514523	-49.47409	0.03067	1801
4690.618201	-49.57756	0.03503	1801
4691.607737	-49.51399	0.04058	1801
4939.845725	-49.43937	0.03486	1801
4940.734595	-49.58375	0.03094	1801
4941.851984	-49.54081	0.02903	1801
4942.695907	-49.47747	0.02271	2701
4942.874690	-49.41960	0.02908	2701
4943.665531	-49.51029	0.02530	2701
4943.887221	-49.58850	0.02681	2701
4944.685781	-49.55404	0.02498	2701
4944.868869	-49.57455	0.02493	2701
4945.696896	-49.54421	0.02523	2701
4945.827736	-49.57673	0.02625	2701
4946.728868	-49.46616	0.02511	2701
4946.906874	-49.45777	0.02557	2701
4947.655776	-49.50278	0.02608	2701
4947.869385	-49.50923	0.02514	2701
4948.641504	-49.52028	0.02507	2701
4948.883575	-49.62500	0.02543	2701
4949.864625	-49.46432	0.02787	2701
4951.666090	-49.52332	0.02495	2701
4951.871943	-49.54578	0.02712	2701
4982.719638	-49.57744	0.04394	1801
4983.784326	-49.47861	0.02903	2701
4985.641154	-49.55333	0.02307	2701
4995.733890	-49.45198	0.02959	2701
5003.534092	-49.55061	0.06991	2701
5003.567956	-49.61140	0.10818	2701
5010.654298	-49.50113	0.04273	2701
5013.621393	-49.46994	0.02968	2701
CORALIE	*Rossiter-McLaughlin effect*		
4972.771828	-49.45006	0.02583	2701
4973.656162	-49.49751	0.03027	1801
4973.681857	-49.48758	0.03160	1801
4973.720561	-49.54121	0.03338	1801
4973.743917	-49.52875	0.03615	1801
4973.767227	-49.52131	0.03342	1801
4973.793073	-49.51045	0.03325	1801
4973.816371	-49.45089	0.03254	1801
4973.839647	-49.43288	0.03681	1801
4973.863142	-49.38687	0.03440	1801
4973.886545	-49.37810	0.03488	1801
4973.909809	-49.52989	0.05071	1801
4974.734674	-49.57918	0.02560	2701
4975.619248	-49.40991	0.03130	2701
4976.737444	-49.46715	0.02672	2701
HARPS	*orbital Doppler shift*		
4564.819485	-49.48835	0.01084	1200
4565.873135	-49.43558	0.00919	1200
4567.851637	-49.53681	0.01048	1200

Table B.6. RV data for WASP-18b.

bjd (- 2 450 000)	RV (km s^{-1})	σ_{RV} (km s^{-1})	t_{exp} (s)
CORALIE	*orbital Doppler shift*		
4359.815630	4.03853	0.01401	1801
4362.673973	3.71230	0.01276	1177
4363.733268	2.28379	0.01041	1177
4655.938244	3.03859	0.00835	1801
4657.938708	4.40045	0.01057	1801
4658.892224	4.52777	0.01116	1801
4660.935178	5.11910	0.00931	1801
4661.926785	4.85226	0.00919	1801
4662.911111	4.53095	0.00918	1801
4760.700356	5.15668	0.00851	1801
4762.730774	4.29008	0.00887	1801
4767.543780	3.01935	0.01029	1801
4767.675234	1.81050	0.00839	1801
4767.845516	1.82182	0.01167	1801
4769.805218	2.49459	0.01015	1801
4770.576633	1.52153	0.01416	1801
4770.715597	2.15763	0.00954	1801
4772.648582	2.66395	0.00907	1801
4772.751819	3.93119	0.00969	1801
4773.599640	2.78436	0.00930	1801
4774.606031	3.60566	0.00918	1801
4775.655139	4.72774	0.00966	1801
4776.562493	4.44656	0.01098	1801
4777.543338	4.74172	0.01146	1801
4778.581020	5.15685	0.00902	1801
4779.621363	4.78250	0.01012	1801
4780.551063	4.85945	0.01085	1801
4781.617770	3.73935	0.00824	1801
4782.631526	2.78257	0.00871	1801
4783.635028	2.14893	0.00884	1801
4825.570049	4.84588	0.00972	1801
4827.645241	4.71715	0.00915	1801
4831.640624	2.24706	0.00887	1801
4836.591194	1.91000	0.00975	1801
4838.557763	2.78064	0.01005	1801
4854.571845	2.89455	0.00919	1801
4857.590403	4.91735	0.01008	1801
HARPS	*Rossiter-McLaughlin effect*		
4699.683362	3.97402	0.00923	600
4699.690445	3.90017	0.00802	600
4699.708200	3.80314	0.01065	600
4699.716083	3.69215	0.01002	600
4699.723467	3.57153	0.00931	600
4699.730400	3.48297	0.00851	600
4699.738236	3.35447	0.00777	600
4699.745817	3.21381	0.00615	600
4699.752994	3.09150	0.00611	600
4699.760517	2.99338	0.00632	600
4699.769476	2.89795	0.00584	600
4699.776640	2.83815	0.00550	600
4699.783967	2.80582	0.00571	600
4699.791282	2.73026	0.00655	600
4699.798863	2.64994	0.00639	600
4699.806028	2.55609	0.00557	600
4699.833413	2.28105	0.00479	600
4699.858483	2.05895	0.00499	600
4699.917420	1.65925	0.00470	600
4702.913698	2.02102	0.00544	600
4704.818564	2.22501	0.00528	300
4706.792686	3.25812	0.00582	1800
4709.781421	4.92900	0.00441	677

Table A.1. Differences between fits of WASP-2b, 4b & 5b. $\chi^2_{\rm reduced}$ has been estimated for the radial velocities only.

WASP-2b

$V \sin I$ Prior	on	off	on	off
$V \sin I$ (km s^{-1})	$1.08^{+0.26}_{-0.31}$	$0.99^{+0.27}_{-0.32}$	$1.02^{+0.28}_{-0.25}$	$0.93^{+0.26}_{-0.30}$
β (°)	154^{+10}_{-12}	153^{+11}_{-15}	145^{+12}_{-15}	143^{+12}_{-18}
e	-	-	$0.035^{+0.016}_{-0.014}$	$0.036^{+0.017}_{-0.015}$
ω (°)	-	-	-103^{+6}_{-12}	-103^{+6}_{-11}
$\chi^2_{\rm RV}$	100.6 ± 12.5	100.5 ± 12.5	93.1 ± 13.6	92.9 ± 13.6
$\chi^2_{\rm reduced}$	2.14 ± 0.27	2.14 ± 0.27	2.07 ± 0.30	2.06 ± 0.30

	no RM	RM fixed	RM fixed	no RM	RM fixed	RM fixed
$V \sin I$ (km s^{-1})	-	1.6	0.9	-	1.6	0.9
β (°)	-	0	0	-	0	0
e	-	-	-	$0.041^{+0.015}_{-0.016}$	$0.044^{+0.016}_{-0.014}$	$0.044^{+0.014}_{-0.016}$
ω (°)	-	-	-	-96^{+5}_{-6}	-98^{+5}_{-6}	-97^{+5}_{-6}
$\chi^2_{\rm RV}$	113.7 ± 15.1	164.0 ± 18.1	135.8 ± 16.5	105.7 ± 14.5	154.0 ± 17.5	126.4 ± 15.9
$\chi^2_{\rm reduced}$	2.32 ± 0.31	3.49 ± 0.39	2.89 ± 0.35	2.25 ± 0.31	3.42 ± 0.39	2.81 ± 0.35

WASP-4b

$V \sin I$ Prior	on	off	on	off
$V \sin I$ (km s^{-1})	$2.14^{+0.38}_{-0.35}$	4^{+46}_{-2}	$2.15^{+0.45}_{-0.39}$	78^{+41}_{-75}
β (°)	-4^{+43}_{-34}	4^{+84}_{-80}	$0.^{+34}_{-41}$	28^{+118}_{-0}
e	-	-	$0.0105^{+0.0036}_{-0.0072}$	$0.0106^{+0.0038}_{-0.0074}$
ω (°)	-	-	-108^{+282}_{-58}	-107^{+280}_{-61}
$\chi^2_{\rm RV}$	77.8 ± 12.5	78.0 ± 12.5	75.3 ± 12.4	75.3 ± 12.3
$\chi^2_{\rm reduced}$	1.69 ± 0.27	1.70 ± 0.27	1.71 ± 0.28	1.71 ± 0.28

WASP-5b

$V \sin I$ Prior	on	off	on	off
$V \sin I$ (km s^{-1})	$3.24^{+0.35}_{-0.27}$	$3.24^{+0.34}_{-0.35}$	$3.32^{+0.30}_{-0.32}$	$3.36^{+0.32}_{-0.46}$
β (°)	$-12.1^{+10.0}_{-8.0}$	$-12.4^{+11.9}_{-8.2}$	$-14.1^{+10.8}_{-7.8}$	$-16.1^{+14.2}_{-9.3}$
e	-	-	$0.0209^{+0.0081}_{-0.0075}$	$0.0209^{+0.0071}_{-0.0087}$
ω (°)	-	-	-137^{+14}_{-16}	-137^{+12}_{-17}
$\chi^2_{\rm RV}$	143.7 ± 17.0	144.3 ± 17.0	136.8 ± 16.5	136.7 ± 16.5
$\chi^2_{\rm reduced}$	3.68 ± 0.44	3.70 ± 0.44	3.70 ± 0.45	3.70 ± 0.45

Table A.2. Differences between fits of WASP-15b, 17b & 18b. $\chi^2_{\mathrm{reduced}}$ has been estimated for the radial velocities only.

WASP-15b

$V \sin I$ Prior	on	off	on	off
$V \sin I$ (km s^{-1})	$4.26^{+0.27}_{-0.32}$	$4.27^{+0.26}_{-0.36}$	$4.37^{+0.29}_{-0.32}$	$4.36^{+0.27}_{-0.34}$
β (°)	$139.8^{+5.1}_{-4.5}$	$139.6^{+5.2}_{-4.3}$	$142.6^{+5.3}_{-4.5}$	$142.7^{+5.3}_{-5.0}$
e	-	-	$0.043^{+0.020}_{-0.022}$	$0.043^{+0.022}_{-0.023}$
ω (°)	-	-	96^{+45}_{-22}	96^{+38}_{-26}
χ^2_{RV}	133.1 ± 16.3	133.3 ± 16.3	130.3 ± 16.1	130.1 ± 16.1
$\chi^2_{\mathrm{reduced}}$	1.57 ± 0.19	1.57 ± 0.19	1.57 ± 0.19	1.57 ± 0.19

WASP-17b

$V \sin I$ Prior	on	off	on	off
$V \sin I$ (km s^{-1})	$9.92^{+0.40}_{-0.45}$	$10.14^{0.58}_{-0.79}$	$9.95^{+0.45}_{-0.43}$	$10.27^{+0.68}_{-0.84}$
β (°)	$148.5^{+5.1}_{-4.2}$	$147.3^{+5.9}_{-5.5}$	$150.9^{+5.2}_{-5.9}$	$150.5^{+6.1}_{5.7}$
e	-	-	$0.062^{+0.024}_{-0.039}$	$0.066^{+0.030}_{-0.043}$
ω (°)	-	-	34^{+34}_{-72}	45^{+30}_{-77}
χ^2_{RV}	190.1 ± 19.5	190.4 ± 19.5	187.3 ± 19.4	186.9 ± 19.3
$\chi^2_{\mathrm{reduced}}$	1.70 ± 0.17	1.70 ± 0.17	1.70 ± 0.18	1.70 ± 0.18

WASP-18b

$V \sin I$ Prior	on	off	on	off
$V \sin I$ (km s^{-1})	$14.04^{+0.73}_{-0.52}$	$14.66^{0.86}_{-0.58}$	$14.67^{+0.81}_{-0.57}$	$15.57^{+1.01}_{-0.69}$
β (°)	$-11.1^{+3.3}_{-2.9}$	$-10.1^{+3.1}_{-2.9}$	$-5.0^{+3.1}_{-2.8}$	$-4.0^{+2.52}_{-2.50}$
e	-	-	$0.0084^{+0.0008}_{-0.0010}$	$0.0085^{+0.0009}_{-0.00010}$
ω (°)	-	-	$-92.8^{+5.2}_{-3.9}$	$-92.1^{+4.9}_{-4.3}$
χ^2_{RV}	283.3 ± 23.8	279.2 ± 23.6	179.7 ± 18.9	177.8 ± 18.9
$\chi^2_{\mathrm{reduced}}$	5.67 ± 0.48	5.58 ± 0.47	3.74 ± 0.39	3.70 ± 0.36